NATIONAL INSTITUTE OF ELECTRICITY AND ELECTRONICS
INELEC - BOUMERDES
DEPARTMENT OF RESEARCH

THESIS

Presented in partial fulfilment of the requirement of the

DEGREE OF MAGISTER

In **Electronic Systems Engineering**

by

Mokrane DEHMAS

EXTENSION OF THE METHOD OF LINES FOR THE ANALYSIS OF SEMICONDUCTOR DEVICES

Defended on December 8, 1996 before the jury:

President: *Dr. A. FARAH, MC, ENP.*

Members: *Dr. H. BOURDOUCEN, MC, INELEC.*
Dr. R. AKSAS, MC, ENP.
Dr. M. T. BELAROUSSI, Chargé de Recherche, CDTA.
Dr. M. BOUMAOUR, Chargé de Recherche, UDTS.

Registration number: 03/96

DEDICATION

I dedicate this work to

the memory of my mother, grand mother and grand father.

my brave father, my family members and my aunt.

all those struggling for peace and freedom.

all the people suffering from diseases and starvation.

ACKNOWLEDGMENTS

I express my sincere and deep gratitude to my supervisor Dr. H. BOURDOUCEN for his guidance and encouragement for the realization of this thesis.

I wish also to express my great appreciation to Dr. A. FARAH (Maître de Conférences, ENP) for his kind acceptance to be president of the jury and his useful discussions and comments. I am equally grateful to Dr. R. AKSAS (Maître de Conférences, ENP), Dr. M. T. BELAROUSSI (Chargé de recherche, CDTA) and Dr. M. BOUMAOUR (Chargé de recherche, UDTS) for examining this thesis and their interesting comments and suggestions.

I would like also to acknowledge the INELEC library and postgraduate staffs for their precious support for the achievement of this work.

I am further grateful to my colleagues postgraduate students for the fruitful discussions and appreciated collaboration and cooperation.

I wish also to express to all the teachers I had during my studies my recognition and distinguished thanks and deep gratitude.

Finally, I express my remarkable and infinite thanks to my father and family members for their patience and continuous encouragement during my studies.

TABLE OF CONTENTS

ABSTRACT

The Method of Lines is a semianalytical technique for numerical simulation of Partial Differential Equations. Although the various advantages of this method such as simplicity in concept, efficiency, and reduced computer memory space and time requirements, its application is still confined in the field of integrated microwave structures.

In this work, a mathematical extension based on this technique, in both equidistant and nonequidistant discretization schemes, is described for two-dimensional solution of Poisson's equation which governs the electrical potential distribution in a semiconductor struture subject to boundary conditions. The developed analysis is then applied to provide solutions for practical problems related to semiconductor devices, followed by a set of illustrative examples and an actual case study.

Chapter 1

INTRODUCTION

The spectacular growth in semiconductor technology during the last few decades has made possible the fabrication of very small size devices with high operating speed and low power consumption. The continuous need to develop new types of semiconductor components with better performances implies a detailed understanding of the physics and an accurate prediction of the behavior and limitations of these devices before fabrication.

Obviously, this can be achieved by providing physical models based on accurate solutions of the set of semiconductor equations which govern the physical phenomenon within these devices. This set consists of linear and nonlinear partial differential equations which are solved subject to prescribed boundary conditions according to the considered physical problem.

Generalized analytical solutions would obviously be optimal for this problem, but, because of the complexity of semiconductor equations, this type of solutions are not available for all devices. However, it is possible to obtain closed-form analytical solutions for some specific device structures by making suitable approximations. A well known example of this type of analysis is described by Shockley in his paper on one-dimensional analysis of unipolar field effect transistors in 1952 [1]. This approach proceeds by dividing the device into regions in which simplifying approximations are applied, joined by an appropriate choice of boundary conditions [1,2]. The majority of closed-form analytical models are restricted to one-dimensional approximation although two-dimensional effects have been considered for some specific device structures and operating conditions [3]. These solutions are more suitable for low frequencies and large geometry devices with predominantly one-dimensional field and

carrier profiles. Although this approach allows rapid analysis because of the straightforward nature of the computer algorithms used to evaluate the closed-form expression and provides a basic insight into the device physics, it is severely limited in the range of applications and accuracy because of nonlinearity and multi-dimensional nature of most modern devices. Hence, this approach is not suitable for modeling sub-micron and planar devices found in discrete and integrated forms where the transport process is multi-dimensional and the electric field varies rapidly throughout the device.

A more generalized approach to overcome these limitations is based on the use of numerical techniques. This approach usually requires considerable computer time but produces more accurate results and flexibility.

Interest in numerical simulation of semiconductor devices using physical device models started in 1964 when Gummel successfully applied it to extract DC characteristics of a silicon bipolar transistor using a one-dimensional steady-state model [4]. Four years later, De Mari described one-dimensional numerical models for *p-n.* junctions [5]. Again, the limited computer resources available at that time restricted device simulations to one-dimension with relatively better accuracy.

To obtain a more realistic representation of planar, three-terminal, and most monolithic integrated circuit devices which are rather surface oriented, two-dimensional numerical models were developed. These models allow important phenomena such as high level injection in bipolar junction transistors, short and thin channel effects in FET's and breakdown effects to be investigated. Kennedy and O'Brien reported a two-dimensional simulation for silicon junction field effect transistors in 1970 [6]. A two-dimensional BJT simulation was described by Slotboom in 1973 [7]. Earlier efforts concentrated on the JFET's [6,8], while a very large number of more recent simulations concerned the MOSFET's [9,10] and MESFET's [11,12] for their fundamental role in integrated circuit technology and high frequency engineering.

Three-dimensional simulations have been recently developed to investigate three-dimensional effects found in very small geometry devices. This type of models has been

used in very large scale of integration (VLSI) MOSFET's to investigate fringing field effects as well as breakdown and threshold voltage variations [13,14].

The increasing effort developed in the field of semiconductor numerical simulation using physical models motivated by the availability of powerful digital computers has led to the development of a set of software packages. Some of these simulators are MINIMOS [15] and CADDET [16] for two-dimensional and WATMOS [13] for three-dimensional MOSFET modeling. However, bipolar simulators include BIPOLE [17] for one-dimensional and BAMBI [18] for two-dimensional models.

The mostly applied numerical techniques to solve semiconductor device equations are finite difference and finite element methods which constitute the basic tools for the development of current packages, and in several numerical simulation tops in a wide variety of engineering fields. These techniques are based on the discretization of the equations across the specified geometrical domain of the device into grids i.e. nodes for finite difference method and small geometry elements for finite element method, and then the resulting algebraic equations are submitted to numerical algorithms which are usually recursive. Although their popularity, these methods present some limitations such as problem of convergence, large time consuming and wide memory space requirement, reason for which packages based on these techniques require, for most applications, work stations to be executed on.

A *seminumerical* approach based on a mathematical method known, as the Method of Lines [19], is proposed in the present work for the analysis of semiconductor devices. This method, first introduced in the field of microwave circuit By R. Pregla and W. Schultz in 1980 [20] and applied by several authors in this field where Laplace's and Helmotz's equations are considered for respectively quasi static and full wave analysis [21-37] of these circuits, has not yet been extended, to the best of our knowledge, for modeling semiconductor devices.

This approach is characterized by its mathematical efficiency and simplicity in concept; for a given partial differential equation subject to appropriate boundary conditions, all

but one of the independent variables are discretized. This equation is then transformed into a set of ordinary differential equations which are solved analytically versus the nondiscretized variable, expressing the solution along *lines* parallel to this variable axis, reason for which it is known as the *Method of Lines* (*MoL*).

This semianalytical scheme makes this technique powerful and efficient in the sense that it provides accurate results with less numerical effort and doesn't face problems of convergence. Moreover, this approach saves time and memory space and this makes it possible to run on widely available AT Personal Computers with average RAM size.

In order to take advantage from these features in the field of semiconductor device modeling, a detailed mathematical extension based on this technique is presented in this document for a two-dimensional simulation of Poisson's equation which governs the electrical potential profile within these components. This can be used to evaluate the depletion capacitance which, when compared to its measured value, gives information about defects in impurity concentrations in the material. Furthermore, an important application of this work is the calculation of the breakdown voltage of devices in reverse biased conditions and MOS structures and, hence, this allows to make optimum designs to meet prescribed breakdown voltages.

After this introductory part, the second chapter of this document provides the basic equations considered in most semiconductor physical modeling topics, with a special interest directed towards Poisson's equation and related materials, since it is the main subject of the remaining analysis. However, chapter three describes the common methods used in this type of modeling. This covers a one-dimensional analytical solution of Poisson's equation and a set of the mostly applied numerical techniques. Chapter four constitutes the main part of this work since it shows in details the mathematical steps involved in the extension of the Method of Lines for the solution of Poisson's equation. A nonless important part of this document is the fifth chapter in the sense that it shows an extension of the developed mathematical tool to provide solutions for practical problems related to semiconductor device configurations. Chapter six is dedicated for the application of the obtained technique for some suitably chosen examples, followed

by a real case study dealing with a potential profile simulation in a MOS capacitor. Finally, the document ends up with a conclusion in which suggestions for further work in this field are provided.

Chapter 2

BASIC SEMICONDUCTOR DEVICE EQUATIONS

This chapter reviews briefly the basic equations used in most semiconductor device physical modeling topics. This concerns mainly current and carrier continuity equations as well as Poisson's equation. Since the objective of the coming analysis is to provide a solution to the latest equation, then all the related materials such as space charge density, boundary and interface conditions are also discussed.

2. 1 Current transport equations:

Current flow in semiconductors can be caused by an applied electric field and a gradient in carrier concentration when maintained different from zero [38]. The first causes *carrier drift,* and the second gives rise to *carrier diffusion.*

2.1.1 Drift current:

This current is due to carrier acceleration caused by an applied electric field. It is composed of electron and hole drift currents . Their densities are respectively given by:

$$J_e = -qn(v_d)_e = +qn\mu_e E \qquad (2.1.a)$$

$$J_h = +qp(v_d)_h = +qp\mu_h E \qquad (2.1.b)$$

where q is the elementary charge. n (p), $(v_d)_{e(h)}$ and $\mu_{e(h)}$ denote respectively the carrier density, the drift velocity and mobility for electrons (holes), and E represents the electric field.

The total drift current, being the sum of the two previous currents, is expressed by:

$$J_{drift} = (J_e + J_h) = q(n\mu_e + p\mu_h)E = q\sigma E \qquad (2.2)$$

where σ denotes the material electrical conductivity which depends strongly on the carrier concentrations.

2.1.2 Diffusion current:

This type of current is created by carrier scattering caused by the gradient in carrier concentrations, that is carriers diffuse from regions of higher to regions of lower densities [39]. Like drift current, this current consists of electron and hole current components, and their densities are respectively,

$$J_e(diff) = +qD_e\nabla n \tag{2.3.a}$$

$$J_h(diff) = -qD_h\nabla p \tag{2.3.b}$$

where ∇n *and* ∇p denote the gradients of electron and hole densities. D_e *and* D_h are the electron and hole diffusion constants which are expressed by the Einstein relationships:

$$D_e = \frac{\mu_e kT}{q} \quad \text{and} \quad D_h = \frac{\mu_h kT}{q} \tag{2.4}$$

where k is the Boltzmann's constant and T the lattice absolute temperature.

When both concentration gradients and electric field are present, the current carried by each type of carriers has two components: drift and diffusion. From eqs. (2.1) and (2.3), their densities are given respectively by;

$$J_e = qn\mu_e E + qD_e\nabla n \tag{2.5.a}$$

$$J_h = qp\mu_h E - qD_h\nabla p \tag{2.5.b}$$

which are known as *current-transport equations*.

Finally the total *conduction current* density J, composed of the electron and hole current density components, is given by:

$$J = J_e + J_h \tag{2.6}$$

2.2 Carrier continuity equations:

These equations govern the change in carrier concentrations in a semiconductor material [40]. To derive a one-dimensional continuity equation for electrons, consider an infinitesimal slice of thickness dx located at x as shown in fig.(2.1). The number of electrons in the slice may increase (decrease) because of the flow into (out) the volume and carrier generation (recombination) within the slab. The overall electron rate of change is the algebraic sum:

(1) The flow into the slab, minus (2) the flow out, plus (3) the rate at which electrons are generated, minus (4) the rate at which they recombine.

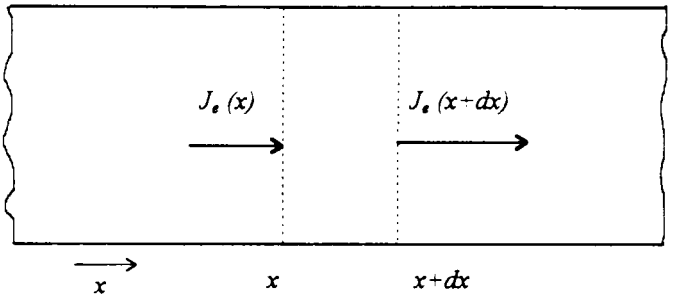

Fig. (2.1) Illustration for the derivation of carrier continuity equations.

The first two components are found by dividing the electron current at each size of the slice by the electron charge. If we symbolize the last two terms respectively by G and R, then the rate of change in the number of electrons in the slab is given by:

$$\frac{\partial n}{\partial t} A\, dx = \left(\frac{J_e(x)}{-q} - \frac{J_e(x+dx)}{-q} \right) A + \left(G_e - R_e \right) A dx \qquad (2.7)$$

where A is the cross sectional area of the slice and, G_e and R_e are respectively the generation and recombination rates of electrons per unit volume. Recombination and generation are processes that happen in a semiconductor material which are defined as follows:

recombination: it is the process in which an electron in the conduction band loses its energy and falls into an empty space in the valence band, resulting in a loss of an electron-hole pair, that is $R_e = R_h$.

generation: it is the opposite process to recombination, that is an electron in the valence band receives enough energy to move into the conduction band creating an electron-hole pair, that is $G_e = G_h$.

If dx in eq. (2.7) is let small, then the basic one-dimensional continuity equation for electrons is expressed as:

$$\frac{\partial n}{\partial t} = \frac{1}{q} \frac{J_e(x)}{\partial x} + \left(G_e - R_e \right) \qquad (2.8)$$

In more than one dimension this equation takes the form:

$$\frac{\partial n}{\partial t} = \frac{1}{q}\nabla . J_e + \left(G_e - R_e\right) \tag{2.9.a}$$

A similar continuity equation can be derived for holes, except that the sign of the first term on the right-hand side is changed because of the charge associated with a hole, that is

$$\frac{\partial p}{\partial t} = -\frac{1}{q}\nabla . J_h + \left(G_h - R_h\right) \tag{2.9.b}$$

2.3 Poisson's equation:

In this section, the remaining basic equation which is mostly used in physical modeling of semiconductor devices is derived [41]. This equation governs the potential profile in a semiconductor material and constitutes the starting point for several analyses in this field.

According to Gauss's law which belong to the set of Maxwell's equations, the electric field flux vector D is related to the electric space charge density ρ, by:

$$\nabla . D = \rho \tag{2.10}$$

D is expressed in terms of the electric field E as:

$$D = \varepsilon\varepsilon_0 E \tag{2.11}$$

where ε_0 and ε denote respectively the dielectric permittivity of vacuum and the relative dielectric constant of the considered material.

In this analysis, the medium is assumed to be homogeneous and isotropic. A *homogeneous* medium is the one for which the quantity ε is constant throughout the medium. It is *isotropic* if ε is a scalar constant, so that D and E have everywhere the same direction.

Combining eqs. (2.10) and (2.11) yields:

$$\nabla . E = \frac{\rho}{\varepsilon\varepsilon_0} \tag{2.12}$$

which describes the divergence of the electric field at any point in space in terms of the space charge density existing at that point.

Since the electric field is related to the scalar potential function by:

$$E = -\nabla\phi \tag{2.13}$$

then eq. (2.12) may be rewritten as,

$$\nabla^2\phi = -\frac{\rho}{\varepsilon\varepsilon_0} \qquad (2.14)$$

This differential equation, known as *Poisson's equation*, relates the potential variation at any point to the charge density at that point, and it is written explicitly in two dimensions as:

$$\frac{\partial^2\phi}{\partial x^2}+\frac{\partial^2\phi}{\partial y^2} = -\frac{\rho}{\varepsilon\varepsilon_0} \qquad (2.15)$$

The solution of this equation in the field of semiconductor modeling requires information about the space charge profile and the boundary conditions of the considered structure which are discussed in the following subsections.

2.3.1 Space charge in a semiconductor:

In a semiconductor material, four types of charged particles may be present:

Positively charged particles:

1. Mobile holes, *p*.
2. Ionized donor atoms, N_d.

Negatively charged particles:

1. Mobile electrons, *n*.
2. Ionized acceptor atoms, N_a.

where the symbols *p*, *n*, N_d and N_a represent the volume concentration of the corresponding particle types. The total space charge density is therefore written as:

$$\rho = q\left(N_d - N_a + p - n\right) \qquad (2.16)$$

The depletion approximation is usually used in the solution of Poisson's equation for reverse biased devices at equilibrium [42]. This approximation divides the semiconductor into distinct regions that are either neutral or fully depleted (empty) of mobile carriers, and they are defined as follows:

a) Neutral region:

In this part of the device, the ionized impurities are neutralized by the corresponding mobile carriers. Therefore, the space charge density in this region, is

$$\rho = q\left(N_d - N_a + p - n\right) = 0 \tag{2.17}$$

and eq. (2.14) reduces to the Laplace's equation:

$$\nabla^2\phi = 0 \tag{2.18}$$

Since, the considered region is neutral and in equilibrium, then the previous equation should give the solution $\phi = cste$, equal to the electrode voltage in contact with this region; otherwise, any drop of potential in this layer will result in an electric field that will cause a charge displacement violating the equilibrium condition and the space charge neutrality in there .

b) Depletion region:

This region is considered to be empty of mobile carriers, that is $p = n = 0$. Therefore, eq. (2.14) takes the form:

$$\nabla^2\phi = -\frac{q}{\varepsilon\varepsilon_0}\left(N_d - N_a\right) \tag{2.19}$$

where N_d =0 for P-type and $N_a = 0$ for N-type materials respectively.

As a consequence for the two previous subsections (a & b), at equilibrium condition, the boundary between the neutral and the depletion layers is located in such away the potential drop in the depletion layer is equal to the applied difference of potential as illustrated in section (3.1).

2.3.2 Boundary conditions:

In addition to the fact that ϕ satisfies eq. (2.14) which accepts an infinite number of solutions, it must also satisfy the prescribed conditions on the external boundaries of the considered device. These boundaries are of the Dirichlet and/or Neumann types, which are described as follows:

a) Dirichlet condition:

Dirichlet condition is applied at the boundaries (usually electrodes) where the potential takes the value of a known voltage V, that is,

$$\phi = V \tag{2.20}$$

b) Neumann condition:

This type of boundaries is applied on free external surfaces. It assumes zero external electric field component since there is no electronic emission, i.e.,

$$\frac{\partial \phi}{\partial n} = 0 \tag{2.21}$$

where the operator ∂/n denotes the gradient component along the unit vector **n** normal to that surface.

2.3.3 Interface conditions:

In a semiconductor structure, Poisson's equation takes different forms in mediums of different dielectric permittivities or charge densities. Interface conditions which are considered in the analysis state that, at the interface of two adjacent media 1 and 2, the potential is continuous and the normal component of the electric field verifies Gauss's law [38], so that:

$$\phi_1 = \phi_2 \tag{2.22}$$

and

$$\varepsilon_1 \frac{\partial \phi_1}{\partial n} - \varepsilon_2 \frac{\partial \phi_2}{\partial n} = Q_s \tag{2.23}$$

where $\varepsilon_{1(2)}$ are the dielectric permittivities of the corresponding media, and the unit vector **n** normal to that interface is pointed to layer 2, and Q_s denotes the interface charge density.

2.4 Conclusion:

The basic equations considered in most physical modeling of semiconductor devices are described throughout this chapter. However, in many analyses dealing with reverse biased devices for the extraction of parameters such as breakdown voltage, the problem reduces to the solution of Poisson's equation.

In order to perform semiconductor device modeling, solutions should be provided for the described equations to fit the specified boundary conditions. For this purpose, several analytical and numerical techniques have been developed, and the next chapter is entirely devoted for the description of the most popular ones among them.

chapter 3

SEMICONDUCTOR DEVICE MODELING TECHNIQUES

The purpose of this chapter is to present some of the mostly used methods for the solution of semiconductor device equations. This includes a detailed one-dimensional analytical solution of Poisson's equation for a potential simulation in a *p-n* junction diode followed by a brief description of a set of numerical methods which are widely used in multi-dimensional device modeling where analytical solutions can not be obtained. A particular attention is however directed towards finite difference and finite element methods for their popularity in this field.

3.1 Analytical method:

Closed-form methods, widely used prior to the advent of digital computers, are usually restricted to one-dimensional analysis by assuming unidirectional field distribution and homogeneous structures. Analytical solutions for semiconductor equations are generally obtained by solving these equations subject to simplifying approximations.

In order to illustrate this approach, a one-dimensional potential profile is derived for a *p-n* junction diode [42]. This example shows a one-dimensional solution of Poisson's equation for which a two-dimensional semianalytical solution is provided in the next chapter.

The physical model of the diode under consideration is shown in fig. (3.1.a). This consists of an interface where the impurity concentration changes from N_a in *P*-type to N_d in *N*-type materials, respectively. Depletion approximation assumes that the depletion region which lies between the positions $-x_p$ and x_n, for now unknown, is completely empty of free carriers. This assumes constant space charge densities in the two layers constituting this region as

illustrated in fig. (3.1.b). However, elsewhere in the bulk, the space charge density is zero since the ionized impurity atoms are neutralized by the corresponding free carriers.

We recall that in the depletion region Poisson's equation takes the form:

$$\frac{\partial^2 \phi}{\partial x^2} = -\frac{q}{\varepsilon\varepsilon_0}\left(N_d - N_a\right) \tag{3.1.a}$$

and, in the neutral regions, it is written as:

$$\frac{\partial^2 \phi}{\partial x^2} = 0 \tag{3.1.b}$$

Integrating eq. (3.1.a), we obtain the expression for the electric field intensity E,

$$E = -\frac{\partial \phi}{\partial x} = \frac{q}{\varepsilon\varepsilon_0}\left(N_d - N_a\right)x + C \tag{3.2}$$

where C denotes the integration constant.

In the P-side of the junction N_d is zero, and on the N-side N_a is zero. Hence, two separate equations for the electric field, one for each side of the depletion area, can be written as:

$$E_n = -\frac{d\phi_n}{dx} = \frac{q}{\varepsilon\varepsilon_0} N_d\, x + C_1, \qquad 0 < x < x_n \tag{3.3.a}$$

and

$$E_p = -\frac{d\phi_p}{dx} = -\frac{q}{\varepsilon\varepsilon_0} N_a\, x + C_2, \qquad -x_p < x < 0 \tag{3.3.b}$$

Since the depletion approximation assumes zero electric field at the edges of the charged region, then

$$E_n = 0 \quad at \quad x = x_n \tag{3.4.a}$$

and

$$E_p = 0 \quad \text{at} \quad x = -x_p \tag{3.4.b}$$

Introducing the above conditions in eqs. (3.3) yields:

$$E_n = -\frac{d\phi_n}{dx} = \frac{q}{\varepsilon\varepsilon_0} N_d \left(x - x_n\right), \qquad 0 < x < x_n \tag{3.5.a}$$

and

$$E_p = -\frac{d\phi_p}{dx} = -\frac{q}{\varepsilon\varepsilon_0} N_a \left(x + x_p\right), \qquad -x_p < x < 0 \tag{3.5.b}$$

At the junction (x=0), the electric field satisfies the interface condition in eq. (2.23). Hence,

$$N_d\, x_n = N_a\, x_p \tag{3.6}$$

This equation verifies the expected result which states that the developed space charge is the same but of opposite sign on the junction sides.

Integrating eqs. (3.5) for the potential, we obtain

$$\phi_n = -\frac{q}{\varepsilon\varepsilon_0} N_d \left(\frac{x^2}{2} - x_n x \right) + C_3 \quad ; \qquad 0 < x < x_n \tag{3.7.a}$$

and

$$\phi_p = \frac{q}{\varepsilon\varepsilon_0} N_a \left(\frac{x^2}{2} + x_p x \right) + C_4 \quad ; \qquad -x_p < x < 0 \tag{3.7.b}$$

with $C_3 = C_4$, resulting from the application of the potential interface condition at the junction (eq. (2.22)).

Since the voltage drop in the neutral layers is approximated to zero, then the difference of potential across the depletion layer is:

$$V = \phi_n(x_n) - \phi_p(-x_p) = \frac{q}{2\varepsilon\varepsilon_0}\left(N_d\, x_n^{\,2} + N_a\, x_p^{\,2} \right) \tag{3.8}$$

Solving simultaneously eqs. (3.6-8) for the depletion layer widths in each side of the junction yields:

$$x_n = \sqrt{\frac{2\varepsilon\varepsilon_0 N_a V}{q N_d \left(N_a + N_d \right)}} \tag{3.9.a}$$

and

$$x_p = \sqrt{\frac{2\varepsilon\varepsilon_0 N_d V}{q N_a \left(N_a + N_d \right)}} \tag{3.9.b}$$

Like eq. (3.6), these equations indicate that the space charge layer penetrates deeper into the region with the lower doping concentration. If, for example $N_d >> N_a$, then $x_p >> x_n$ and the total depletion width simplifies to

$$d = x_n + x_p \approx x_p \tag{3.10}$$

and the total voltage V across the depletion region is:

$$V = V_a + V_{bi} \tag{3.11}$$

where V_{bi} denotes the built-in potential at the junction [42], and V_a is the applied external voltage as shown in fig. (3.1.a).

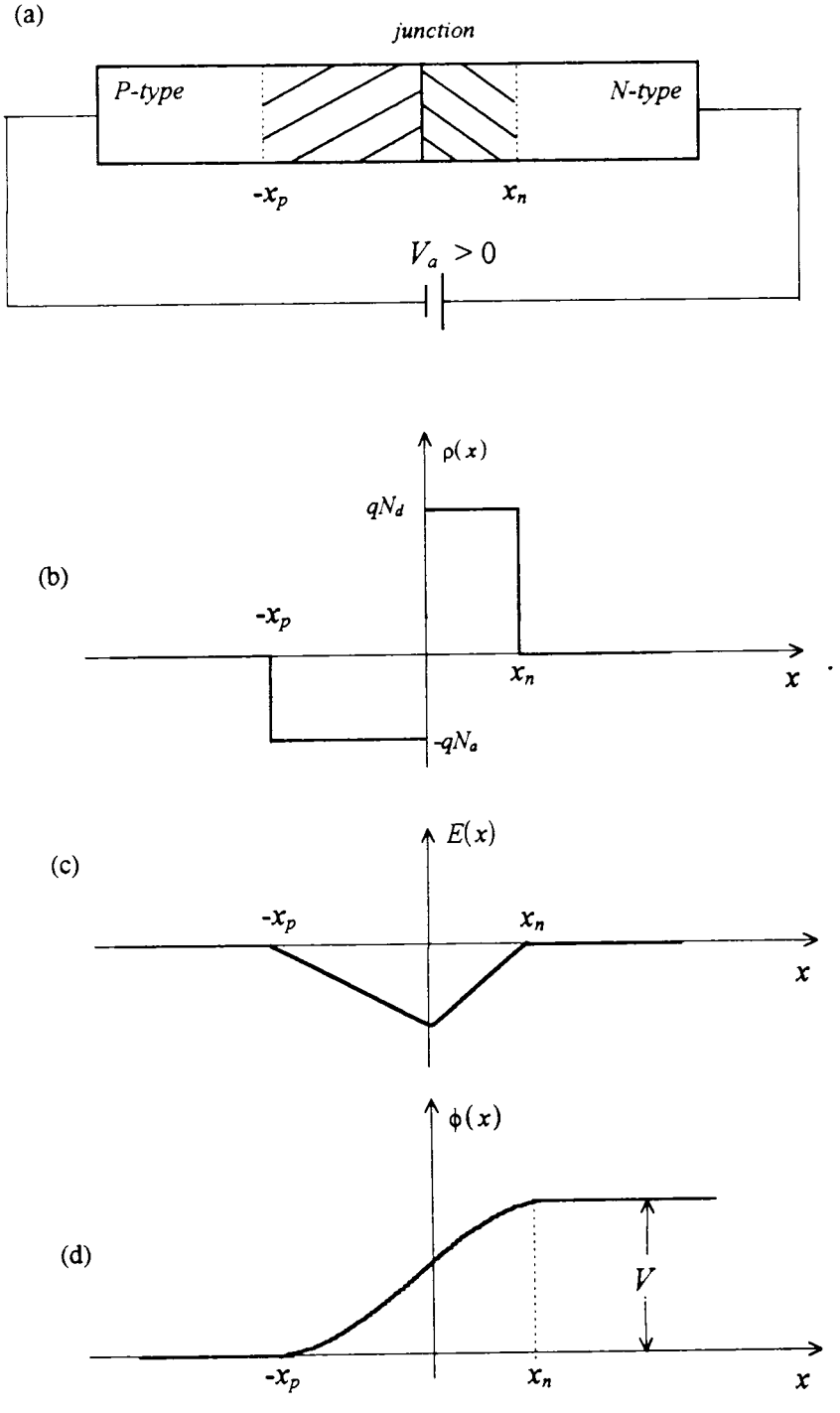

Fig. (3.1) Abrupt reverse biased *p-n* junction diode. (a) Physical model representation, (b) space charge density, (c) electric field and, (d) electric potential profiles.

3.2 Numerical methods:

Although one-dimensional analysis provides information about the device behavior, this type of modeling is inadequate for most modern devices in which the field distribution is rather multi-dimensional. Since analytical solutions are generally impossible to obtain for multi-dimensional analyses, several numerical techniques have been developed for this purpose. Among these methods, we list the finite difference, finite element and Monte Carlo methods which are described briefly in the following sections.

3.2.1 Finite difference method:

Finite difference method has been widely used to solve discretized semiconductor equations, and continues to be a popular choice in device simulations [4,18]. The reason for this is the availability of considerable information about this method [38,43], and the additional complexity introduced into simulation algorithms by alternative techniques.

The principle of this method consists in subdividing the simulation domain into rectangular meshes, called *grids*, as shown in fig. (3.2) below:

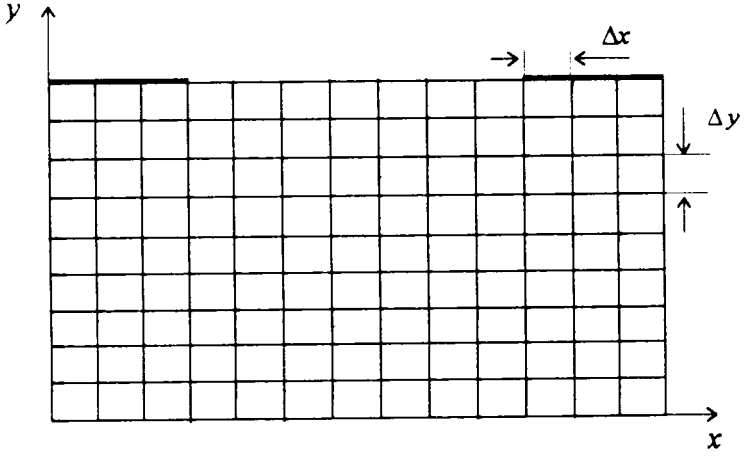

Fig. (3.2) Uniform finite difference mesh.

At the nodes of these grids, called *grid points*, the continuous derivatives in the equations are replaced by discretized finite difference approximations, and solutions for physical variables are produced.

The finite difference equations are derived from truncated Taylor series. For example, for the following Poisson's equation:

$$\nabla^2\phi(x,y) = \frac{\partial^2\phi(x,y)}{\partial x^2} + \frac{\partial^2\phi(x,y)}{\partial y^2} = -\frac{\rho(x,y)}{\varepsilon} \tag{3.12}$$

the second order difference approximation of $\phi(x,y)$ with respect to x is obtained when truncating the series after the second term by proceeding as follows:

$$\phi(x+\Delta x,y) = \phi(x,y) + \frac{1}{1!}\Delta x\frac{\partial\phi(x,y)}{\partial x} + \frac{1}{2!}\Delta x^2\frac{\partial^2\phi(x,y)}{\partial x^2} \tag{3.13.a}$$

and

$$\phi(x-\Delta x,y) = \phi(x,y) - \frac{1}{1!}\Delta x\frac{\partial\phi(x,y)}{\partial x} + \frac{1}{2!}\Delta x^2\frac{\partial^2\phi(x,y)}{\partial x^2} \tag{3.13.b}$$

Adding (3.13.a) and (3.13.b) yields

$$\frac{\partial^2\phi(x,y)}{\partial x^2} = \frac{\phi(x-\Delta x,y) - 2\phi(x,y) + \phi(x+\Delta x,y)}{\Delta x^2} \tag{3.14.a}$$

Similarly, the second order difference approximation of $\phi(x,y)$ with respect to y is

$$\frac{\partial^2\phi(x,y)}{\partial y^2} = \frac{\phi(x,y-\Delta y) - 2\phi(x,y) + \phi(x,y+\Delta y)}{\Delta y^2} \tag{3.14.b}$$

where Δx and Δy are the discretizing step intervals respectively along x and y directions.

Substituting the expressions (3.14) in eq.(3.12), then Poisson's equation is approximated at a grid point (x,y) by:

$$\frac{\phi(x-\Delta x,y) - 2\phi(x,y) + \phi(x+\Delta x,y)}{\Delta x^2} + \frac{\phi(x,y-\Delta y) - 2\phi(x,y) + \phi(x,y+\Delta y)}{\Delta y^2} = -\frac{\rho(x,y)}{\varepsilon} \tag{3.15}$$

It follows that the potential $\phi(x,y)$ at a node (x,y) can be expressed in terms of the potentials at the surrounding nodes. Consequently, if we let ϕ_A, ϕ_B , ϕ_C and ϕ_D to be the potential values at the four neighboring points to the point **P** shown in fig. (3.3), then the potential at **P** can be written as,

$$\varphi_P = a_1\phi_A + a_2\phi_B + a_3\phi_C + a_4\phi_D + a_5\rho_P \tag{3.16}$$

where ρ_P denotes the space charge density at **P**, and the coefficients $a_i's$ are identified when extracting $\phi(x,y)$ from eq. (3.15).

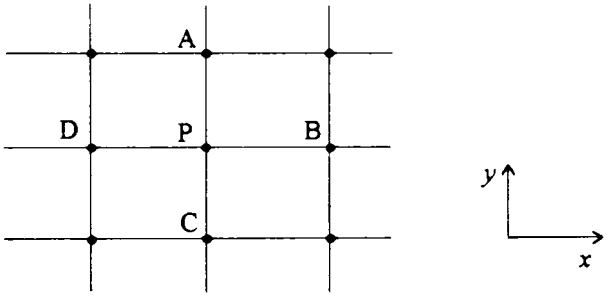

Fig. (3.3) Illustration of the points used in the expression of ϕ_P in eq. (3.16).

An approach to solve the finite difference equation is based on the relaxation method. In this technique, assumed potential values are first assigned to the grid points and modified iteratively as

$$\phi_P^{i+1} = \phi_P^i - \alpha R_P^i \tag{3.17}$$

where i is the iteration number, α the chosen relaxation parameter and R_P^i the residual which represents the difference between ϕ_P^i and the value given by eq. (3.16).

The iterative process is carried out until a specified accuracy is reached, that is when the difference between the values obtained from the last two iterations is less than the allowed error.

Finally, finite difference method suffers from some disadvantages such as large time and memory space requirements in addition to problems of convergence which is not always assured.

3.2.2 Finite element method:

Finite element method is developed in the early 1940's for use in civil and mechanical engineering. The application of this method in semiconductor device modeling was first reported in literature in the 1970's [44, 45]. This technique provides a flexible means for solving semiconductor equations over devices with complex geometry [38].

The first step of this method consists in approximating the solution for the differential equation by simple functions over small geometry elements of the total simulation domain. The total solution is then built up by matching together the solutions in individual elements. In two dimensions, the domain may be subdivided into triangles as shown in fig. (3.4).

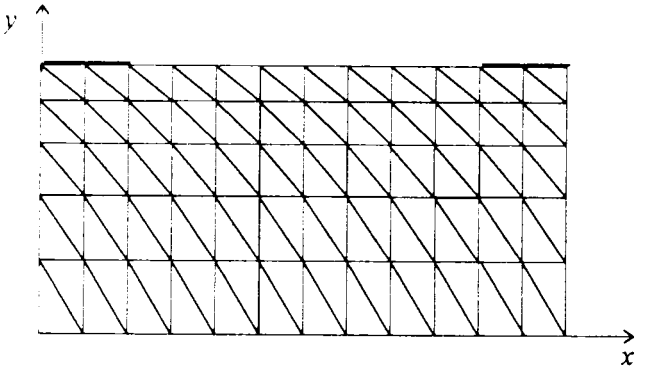

Fig. (3.4) Finite element subdivision of the simulation domain into nonuniform triangular elements.

The solution in an element is usually approximated by a low order polynomial. For example, for Poisson's equation, the potential may be approximated by a function such as:

$$\phi_{element} = a_0 + a_1 x + a_2 y \tag{3.18}$$

When using finite element method, a special significance is attached to the solution at certain points on the elements called *nodes*. For triangular elements, it is adequate to take the nodes at the corners of the triangle as illustrated in fig. (3.5) below:

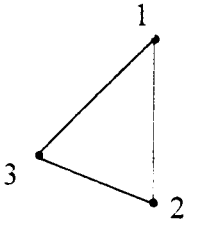

Fig. (3.5) A triangular element with three nodes.

If the values of ϕ at the nodes are respectively ϕ_1, ϕ_2 and ϕ_3 then eq. (3.18) can be rewritten as:

$$\phi_{element} = \sum_{i=1}^{3} N_i(x,y)\,\phi_i \tag{3.19}$$

The functions $N_i(x,y)$ are called *shape functions* and have an equivalent form to the expression in eq. (3.18). Their coefficients are evaluated when assigning to N_i the property of taking the value 1 at the i^{th} node and zero at the others, and therefore we will be left with only ϕ_i's as unknowns.

Substituting the trial function ($\phi_{element}$ in eq (3.19)) into Poisson's equation (3.12) yields:

$$\sum_{i=1}^{3} \phi_i\, \nabla^2 N_i + \frac{\rho}{\varepsilon} = R \tag{3.20}$$

The residual R would be zero if the approximation in eq. (3.18) were exact solution, but in general it will not be, giving rise to an error. The aim is, now, to find the nodal potential values that minimize R and verify the expression of the solutions in all the surrounding elements. For this purpose, several techniques such as the Rayleigh Ritz and Galerkin methods were developed [46].

Although finite element method can be applied for modeling devices with complex geometry, its principle disadvantages are great density of the matrix equations, programming complexity and problems of convergence.

3.2.3 Monte Carlo technique:

Monte Carlo method is a statistical numerical technique for solving mathematical and physical problems. This method has been applied to solve a wide variety of problems before being introduced in the field of semiconductor device modeling by Kurosawa in 1966 [47].

This method solves semiconductor equations using a statistical approach by following the transport history of one or more carriers subject to forces due to applied electric and magnetic fields [38]. Because of this particular scheme, this approach is sometimes considered to be similar to experimental techniques.

The principle of this method consists in following the motion of electrons in the material where random numbers control the scattering process. The motion of each electron is

modeled as a sequence of free flights between successive events (collisions) during which it is accelerated by the existing fields, and obeys the classical laws of motion. The information obtained from these flights is then used to determine the required parameters from simulation. In the case of steady-state modeling, a single particle is considered and the time history must be long enough so that the choice of initial conditions does not influence the final outcome, whereas transient simulation requires the motion of a large number of particles.

This method which is suitable when hot electron effect is considered, requires large execution time and needs detailed knowledge about the system in terms of material parameters as well as the different physical phenomenon involved in the process.

3.3 Conclusion:

Numerical methods constitute the unique alternative for the solution of the most semiconductor device problems. However, they present some limitations such as large memory space requirements, time consuming and problems of convergence. For these reasons, efforts are carried out to develop algorithms that solve all or some of these problems. For the same purpose, a semianalytical technique is provided in the next chapter for the solution of Poisson's equation.

Chapter 4

SOLUTION OF POISSON'S EQUATION BY THE METHOD OF LINES

The semianalytical method of lines is developed by W. Fadeeva for the solution of partial differential equations (PDE's) [19]. This technique was first introduced in the field of engineering for the analysis of microwave circuits where Laplace's and Helmotz's equations given by:

$$\nabla^2\phi = 0 \tag{4.1}$$

and

$$\nabla^2\phi + k^2\phi = 0 \tag{4.2}$$

where k is a scalar, are solved respectively for quasi-static and full-wave analyses [20-37].

Although the various advantages of this technique, its application is still confined in this field. To take advantage from its features in the field of semiconductor device modeling, a detailed mathematical extension based on this technique is provided in this chapter for a two-dimensional solution of the Poisson's equation:

$$\nabla^2\phi = -\rho/\varepsilon \tag{4.3}$$

which controls the potential distribution within these devices.

This operation is achieved by the extension of the scheme already applied for the solution of the Laplace's equation (4.1) in two dimensions, to solve the Poisson's equation (4.3) by a suitable handling of the right hand side of this equation which is no more identical to zero [48]. Moreover, this chapter describes in details all the steps involved in the application of this technique.

4.1 Qualitative description:

The method of lines, very well suited for the analysis of planar structures is characterized by its mathematical efficiency and simplicity in concept; for a given partial differential equation subject to boundary conditions, all but one of the independent variables are discretized [21,24,29]. The discrete variables should be well chosen to benefit from the efficiency of this method. This seminumerical approach transforms a PDE into a set of decoupled ordinary differential equations. The solution is then expressed analytically versus the non-discretized variable, along lines parallel to this variable axis. As expected, the semianalytical scheme of this approach saves considerable amount of time and memory space compared to other purely numerical techniques.

In the following, the analysis is first carried out by letting equidistant discretization, and then the general case of nonuniform discretization is assumed.

4.2 Equidistant discretization:

Let's use the Method of Lines with uniform discretization to solve the two-dimension Poisson's equation:

$$\frac{\partial^2\phi(x,y)}{\partial x^2}+\frac{\partial^2\phi(x,y)}{\partial y^2}=-\frac{\rho(x,y)}{\varepsilon}=f(x,y) \tag{4.4}$$

in the domain shown in fig. (4.1) and subject to boundary conditions that will be discussed latter on. The different steps involved in the analysis are as follows:

4.2.1 Discretization:

If we discretize the variable x and keep y continuous then the functions $\phi(x,y)$ and $f(x,y)$ are transformed to the sets of functions $\phi(x_i,y)$ and $f(x_i,y)$ along the lines:

$$x = ih \quad ; \quad i = 1, 2, \ldots, N.$$

where N is the total number of lines crossing the structure and h the discretizing interval size, as illustrated in fig. (4.1).

This operation transforms eq. (4.4) into a system of N differential equation of the form:

$$\left.\frac{\partial^2\phi(x,y)}{\partial x^2}\right|_{x_i}+\frac{\partial^2\phi(x_i,y)}{\partial y^2}=f(x_i,y) \tag{4.5}$$

If we let

$$\phi(x_i, y) = \phi_i(y) = \phi_i \tag{4.6.a}$$

and

$$f(x_i, y) = f_i(y) = f_i \tag{4.6.b}$$

then, the i^{th} difference approximation with respect to x is expressed as:

$$\left.\frac{\partial \phi}{\partial x}\right|_i = \frac{\phi_{i-1} - \phi_i}{h} + O(h) \quad ; \; i = 0, \ldots, N \tag{4.7}$$

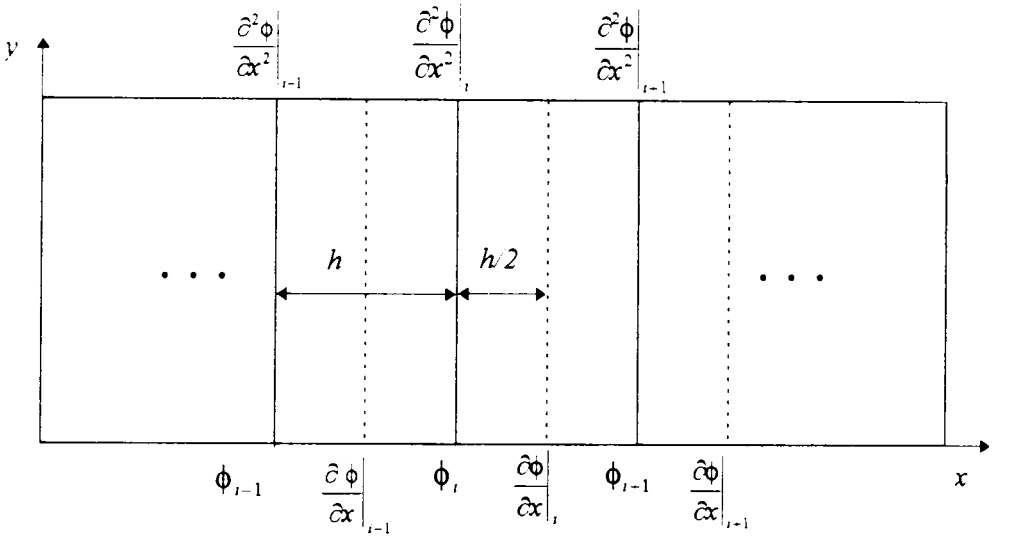

Fig. (4.1) Considered domain and equidistant discretization pattern for the method of lines.

On the same basis, the second partial derivative is approximated by:

$$\left.\frac{\partial^2 \phi}{\partial x^2}\right|_i = \frac{\left.\frac{\partial \phi}{\partial x}\right|_i - \left.\frac{\partial \phi}{\partial x}\right|_{i-1}}{h} + O(h^2) \quad ; \; i = 1, \ldots, N \tag{4.8}$$

In the previous equations $O(h)$ and $O(h^2)$ denote the error terms. Combining eqs. (4.7) and (4.8), and neglecting these terms yields:

$$\left.\frac{\partial^2 \phi}{\partial x^2}\right|_i = \frac{\phi_{i-1} - 2\phi_i + \phi_{i-1}}{h^2} \tag{4.9}$$

For different *i*'s, eq. (4.9) is written as:

$$\left.\frac{\partial^2\phi}{\partial x^2}\right|_1 = \frac{\phi_0 - 2\phi_1 + \phi_2}{h^2} \quad , \ i = 1 \qquad (4.10.a)$$

$$\left.\frac{\partial^2\phi}{\partial x^2}\right|_2 = \frac{\phi_1 - 2\phi_2 + \phi_3}{h^2} \quad , \ i = 2 \qquad (4.10.b)$$

$$\left.\frac{\partial^2\phi}{\partial x^2}\right|_3 = \frac{\phi_2 - 2\phi_3 + \phi_4}{h^2} \quad , \ i = 3 \qquad (4.10.c)$$

$$\vdots \qquad \vdots \qquad \vdots$$

$$\left.\frac{\partial^2\phi}{\partial x^2}\right|_N = \frac{\phi_{N-1} - 2\phi_N + \phi_{N+1}}{h^2} \quad , \ i = N \qquad (4.10.d)$$

which represents a system of N coupled differential equations with $(N-2)$ unknowns (ϕ_0, ϕ_1,..., ϕ_{N+1}).

4.2.2 Lateral boundaries:

The unknowns ϕ_0 and ϕ_{N+1}, appearing in the above system respectively for $i=1$ and $i=N$, are eliminated when considering the lateral boundary conditions. The left boundary is considered in what follows, and the same approach applies for the right hand side. These conditions are of the *Dirichlet* and *Neumann* types;

a) Dirichlet condition:

Dirichlet boundary (fig. (4.2.a)) requires $\phi_0 = 0$. Inserting this condition into eq. (4.10.a) yields:

$$\left.\frac{\partial^2\phi}{\partial x^2}\right|_1 = \frac{-2\phi_1 + \phi_2}{h^2} \qquad (4.11.a)$$

b) Neumann condition:

This condition assumes $\left.\frac{\partial\phi}{\partial x}\right|_0 = 0$ which implies $\phi_0 = \phi_1$ from eq.(4.7). Accordingly, eq. (4.10.a) takes the form:

$$\left.\frac{\partial^2\phi}{\partial x^2}\right|_1 = \frac{-\phi_1 + \phi_2}{h^2} \qquad (4.11.b)$$

Consequently, in both boundary types ϕ_0 is eliminated from eq. (4.10.a). Similarly, the condition on the right lateral side of the domain in fig. (4.1) eliminates ϕ_{N+1} from eq. (4.10.d).

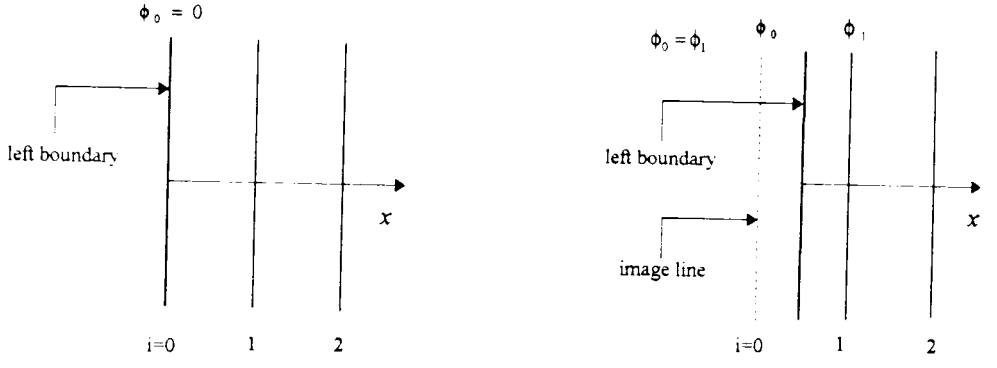

(a) Dirichlet boundary

(b) Neumann boundary

Fig. (4.2) Illustration of Lateral boundary condition types.

If, now, we let the vectors ϕ, f and ϕ_{xx} to be respectively:

$$\phi = (\phi_1, \phi_2, \ldots, \phi_N)^t \tag{4.12.a}$$

$$f = (f_1, f_2, \ldots, f_N)^t \tag{4.12.b}$$

and

$$\phi_{xx} = \left(\left.\frac{\partial^2 \phi}{\partial x^2}\right|_1, \left.\frac{\partial^2 \phi}{\partial x^2}\right|_2, \ldots, \left.\frac{\partial^2 \phi}{\partial x^2}\right|_N \right)^t \tag{4.12.c}$$

then the system (4.10) takes the matrix form:

$$\phi_{xx} = \frac{1}{h^2} P\phi \tag{4.13}$$

with P being the second order difference operator which is an NxN real-symmetric and tridiagonal matrix of the form:

$$P = \begin{bmatrix} p_1 & 1 & & & \\ 1 & -2 & 1 & & \\ & 1 & \ddots & \ddots & \\ & & \ddots & -2 & 1 \\ & & & 1 & p_2 \end{bmatrix} \tag{4.14}$$

where p_1 and p_2 depend on the lateral boundaries. Accordingly, from eqs. (4.11) we get:

a) Dirichlet condition: ϕ_0 and / or $\phi_{N-1} = 0 \Rightarrow p_1$ and /or $p_2 = -2$.

b) Neumann condition: $\left.\frac{\partial\phi}{\partial x}\right|_0$ and / or $\left.\frac{\partial\phi}{\partial x}\right|_N = 0 \Rightarrow p_1$ and /or $p_2 = -1$.

Inserting (4.13) in eq. (4.5), then this one takes the matrix form:

$$\frac{d^2\phi}{dy^2} + \frac{1}{h^2} P\phi = f \tag{4.15}$$

4.2.3 Domain transformation:

Up to this stage, eq. (4.4) is transformed to the system of N coupled differential equations (4.15). For this purpose, the matrix P must be diagonalized by a suitable transformation. This is performed using the linear algebra theorem [49] which states that any real symmetric matrix $\boldsymbol{P}$ is similar to a diagonal matrix λ, i.e., there exist a matrix T such that

$$T^t P T = \lambda \tag{4.16}$$

where the elements λ_i are the eigenvalues of P, T is an orthogonal matrix whose columns are the eigenvectors of P, and T^t its transpose which satisfy the relationship:

$$T^t T = I \tag{4.17}$$

where I is the identity matrix of the same size. Moreover, for the particular tridiagonal matrix P in eq. (4.14), the elements of λ and T can be expressed analytically [29], and their respective forms are shown in appendix **A**.

The above result allows the system (4.15) to be decoupled by premultiplying its both sides by T^t, and obtain

$$\frac{d^2(T^t\phi)}{dy^2} + \frac{1}{h^2} T^t P \underbrace{(TT^t)}_{I}\phi = T^t f \tag{4.18.a}$$

which is equivalent to

$$\frac{d^2(T^t\phi)}{dy^2}+\frac{1}{h^2}(T^tPT)(T^t\phi)=T^tf \qquad (4.18.b)$$

or simply,

$$\frac{d^2V}{dy^2}+\frac{1}{h^2}\lambda V=F \qquad (4.18.c)$$

where V is the transformed vector of potentials and F the transform of f, given respectively by:

$$V=T^t\phi \qquad (4.19.a)$$

and

$$F=T^tf \qquad (4.19.b)$$

4.2.4 General solution:

Now that the system is decoupled and takes the form (4.18.c) in the transformed domain, it can be solved by proceeding as follows:

If we let

$$\lambda_i=-\chi_i^2 \qquad (4.20)$$

then eq. (4.18.c) is expressed as a set of independent equations of the form:

$$\frac{d^2V_i}{dy^2}-\left(\frac{\chi_i}{h}\right)^2V_i=F_i \;; \qquad i=1,\ 2,\ \ldots,\ N \qquad (4.21)$$

The general solution of each of these equations includes a homogeneous part and a particular one, and they are obtained as follows:

a) Homogeneous solution:

The homogeneous solution is obtained when letting the right side of the equation to be zero. For this type of ordinary differential equations, this solution takes the form:

$$V_{H_i}=A_i\cosh\left(\frac{\chi_i}{h}\right)y+B_i\sinh\left(\frac{\chi_i}{h}\right)y \qquad (4.22)$$

where A_i and B_i are arbitrary constants.

b) Particular solution:

Among the available procedures to determine the particular solution we suggest the method of undetermined coefficients in which the general form of this solution is expressed as a linear combination of F_i and its linearly independent derivatives, that is,

$$V_{P_i} = a_{i_0} F_i + a_{i_1} F_i^{(1)} + a_{i_2} F_i^{(2)} + \cdots + a_{i_m} F_i^{(m)} + \cdots \tag{4.23}$$

where $F_i^{(m)}$ denotes the m^{th} derivative of F_i , and the coefficients a_i's are determined when substituting V_i in eq. (4.21) by the expression of V_{P_i} [49].

Furthermore, since F_i depends on the doping profile which is usually constant, linear or an exponential function of y, then its expression involves at most the first two term in eq. (4.23) which can be evaluated easily.

Consequently, the general solution in the transformed domain takes the form:

$$V_i = V_{H_i} + V_{P_i} = A_i \cosh\left(\frac{\chi_i}{h}\right) y + B_i \sinh\left(\frac{\chi_i}{h}\right) y + V_{P_i} \tag{4.24}$$

where the coefficients A_i and B_i are determined when considering the transformed boundary conditions on the horizontal top and bottom surfaces of the device.

At last, to get the vector of potentials ϕ, the vector V must be transformed back to the original domain by the inverse transformation:

$$\phi = TV \tag{4.25}$$

expressing the solutions along the discretization lines in terms of y.

Finally, It has to be noted that in the case of Neumann-Neumann lateral boundaries, one eigenvalue is zero (λ_1 in appendix A), and the solution of the corresponding equation in (4.21) results from a double integration.

4.3 Nonequidistant discretization:

In any numerical modeling of physical phenomenon, there may be regions of the device where the investigated parameter changes strongly and others where it is quiet constant. For accurate results with less numerical efforts, in finite element and finite difference methods,

small size elements and meshes are assumed in the first regions, and let larger in the second ones. Similarly, improved accuracy may be obtained with the method of lines by performing nonequidistant discretization and proceed as follows:

4.3.1 Discretization:

Nonuniform discretization is applied for the structure in fig. (4.3) in which Poisson's equation is solved. In this example, arbitrary disposition of the lines is considered, but in a practical case, the distance between them is selected according to the expected field concentration.

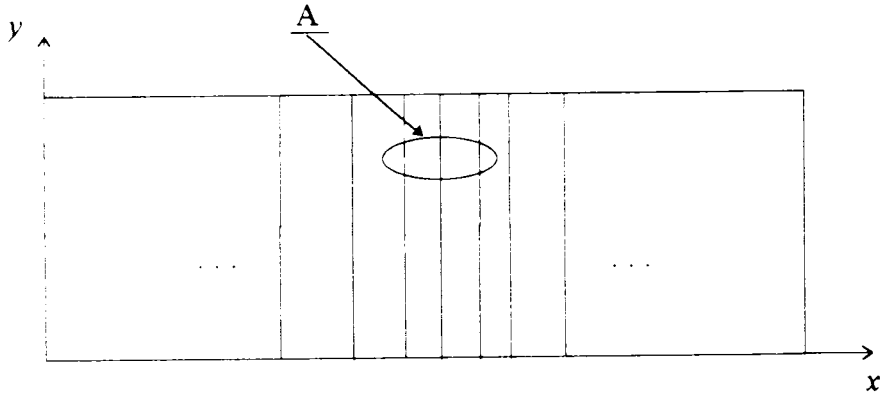

Fig. (4.3.a) Nonequidistant discretization pattern for the method of lines.

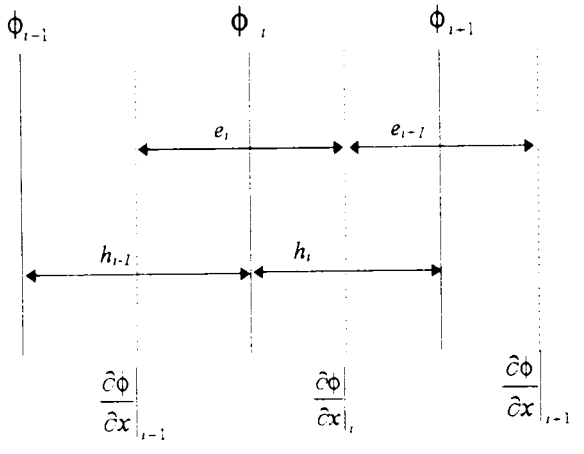

Fig. (4.3.b) Detail A in fig. (4.3.a).

Similarly to uniform discretization, eq. (4.4) is transformed into a set of N equations such as,

$$\left.\frac{\partial^2\phi(x,y)}{\partial x^2}\right|_{x_i} + \frac{\partial^2\phi(x_i,y)}{\partial y^2} = f(x_i,y) \tag{4.26}$$

With the same abbreviations in eqs. (4.6), the i^{th} finite difference approximation is now expressed as,

$$\left.\frac{\partial\phi}{\partial x}\right|_i = \frac{\phi_{i-1}-\phi_i}{h_i} \quad ; \quad i = 0,\ 1,\ \ldots,\ N. \tag{4.27}$$

and the second derivative evaluated on the potential line is:

$$\left.\frac{\partial^2\phi}{\partial x^2}\right|_i = \frac{\left.\frac{\partial\phi}{\partial x}\right|_i - \left.\frac{\partial\phi}{\partial x}\right|_{i-1}}{e_i} \quad ; \quad i = 1,\ 2,\ \ldots,\ N. \tag{4.28}$$

where $e_i = (h_i + h_{i-1})/2$ denotes the i^{th} interval size between dotted lines in fig. (4.3.b).

4.3.2 Normalization:

To obtain a symmetric operator like in the case of equidistant discretization (P), eq. (4.27) is first normalized by multiplying its both sides by $h\sqrt{h_i/h}$ and obtain:

$$h\sqrt{\frac{h_i}{h}}\left(\left.\frac{\partial\phi}{\partial x}\right|_i\right) = \sqrt{\frac{h}{h_i}}\left(-\phi_i + \phi_{i-1}\right) \quad ; \quad i = 0,\ 1,\ \ldots,\ N. \tag{4.29}$$

where h is the assumed normalized discretization interval.

With Dirichlet-Dirichlet lateral conditions, i.e., $\phi_0 = \phi_{N-1} = 0$, the above equations take the matrix form:

$$h r_h^{-1}\phi_x = r_h D\phi \tag{4.30}$$

where

$$r_h = diag\left(\sqrt{\frac{h}{h_i}}\right) \quad ; \quad i = 0,\ 1,\ldots,\ N. \tag{4.31}$$

$$\phi = \left(\phi_1,\ \phi_2,\ \ldots,\ \phi_{\cdot}\right)^t \tag{4.32}$$

and

$$\phi_x = \left(\left.\frac{\partial\phi}{\partial x}\right|_0,\ \left.\frac{\partial\phi}{\partial x}\right|_1,\ \ldots,\ \left.\frac{\partial\phi}{\partial x}\right|_N\right)^t \tag{4.33}$$

whereas the $(N+1)xN$ matrix D is the first order difference operator given by:

$$D = \begin{bmatrix} 1 & & & \\ -1 & 1 & & \\ & -1 & \ddots & \\ & & \ddots & 1 \\ & & & -1 \end{bmatrix} \tag{4.34}$$

Similarly, the second order difference equation (4.28) is normalized by premultiplying it by $h\sqrt{e_i / h}$ and get

$$h\sqrt{\frac{e_i}{h}}\left(\frac{\partial^2\phi}{\partial x^2}\bigg|_i\right) = \sqrt{\frac{h}{e_i}}\left(\frac{\partial\phi}{\partial x}\bigg|_i - \frac{\partial\phi}{\partial x}\bigg|_{i-1}\right) \quad ; \quad i = 1, 2, \ldots, N. \tag{4.35}$$

which takes the matrix form:

$$hr_e^{-1}\phi_{xx} = -r_e D^t \phi_x \tag{4.36}$$

where

$$r_e = diag\left(\sqrt{\frac{h}{e_i}}\right) \quad ; \quad i = 1, 2, \ldots, N. \tag{4.37}$$

and

$$\phi_{xx} = \left(\frac{\partial^2\phi}{\partial x^2}\bigg|_1, \frac{\partial^2\phi}{\partial x^2}\bigg|_2, \ldots, \frac{\partial^2\phi}{\partial x^2}\bigg|_N\right)^t \tag{4.38}$$

whereas the matrix D^t is the transpose of D.

If we extract ϕ_x from eq. (4.30) and insert it into eq. (4.36) we obtain:

$$h^2 r_e^{-1}\phi_{xx} = -\left(r_e D^t r_h\right)\left(r_h D r_e\right)\left(r_e^{-1}\phi\right) \tag{4.39}$$

If we let

$$D_x = r_h D r_e \tag{4.40}$$

and

$$D_{xx} = -D_x{}^t D_x \tag{4.41}$$

then eq (4.39) can be written as

$$h^2 r_e^{-1}\phi_{xx} = D_{xx}\left(r_e^{-1}\phi\right) \tag{4.42}$$

Extracting ϕ_{xx} from the above equality and inserting it into the discretized Poisson's equation (4.26) yields:

$$\frac{d^2\phi}{dy^2} + \frac{1}{h^2} r_e D_{xx}\left(r_e^{-1}\phi\right) = f \tag{4.43}$$

where f is a vector which results from the discretization of $f(x,y)$.

Premultiplying both sides of the previous equation by r_e^{-1}, then this one takes the form:

$$\frac{d^2\psi}{dy^2} + \frac{1}{h^2} D_{xx}\psi = G \tag{4.44}$$

where

$$\psi = r_e^{-1}\phi \tag{4.45}$$

and

$$G = r_e^{-1} f \tag{4.46}$$

being the normalized vectors.

4.3.3 Domain transformation:

Again, D_{xx} is a tridiagonal matrix and the system (4.44) needs to be decoupled before being solved. However, since it is a real-symmetric matrix, then this can be achieved by the orthogonal transformation:

$$T^t D_{xx} T = \lambda \tag{4.47}$$

where the elements λ_i of the diagonal matrix λ are the eigenvalues of D_{xx} and T is the matrix of eigenvectors which satisfies the relation $T^t T = I$ [49].

Premulitiplying the system (4.44) by T^t yields:

$$\frac{d^2\left(T^t\Psi\right)}{dy^2} + \frac{1}{h^2}\left(T^t P T\right)\left(T^t\Psi\right) = T^t G \tag{4.48}$$

or simply,

$$\frac{d^2 V}{dy^2} + \frac{1}{h^2}\lambda V = F \tag{4.49}$$

where

$$F = T^t G \tag{4.50}$$

whereas the vector

$$V = T^t \Psi \tag{4.51}$$

denotes the transform of the normalized vector of potentials

Assuming $\lambda_i = -\chi_i^2$ then eq.(4.42) is further transformed into the set of N ordinary differential equations:

$$\frac{d^2 V_i}{dy^2} - \left(\frac{\chi_i}{h}\right)^2 V_i = F_i \tag{4.52}$$

4.3.4 General solution:

The previous set of equations is similar to the set in eq. (4.21) obtained for uniform discretization. Therefore, the general solution involve homogeneous and particular parts, and it is given by:

$$V_i = A_i \cosh\left(\frac{\chi_i}{h}\right) y + B_i \sinh\left(\frac{\chi_i}{h}\right) y + V_{P_i} \tag{4.53}$$

where A_i and B_i are constants depending on the horizontal sides boundaries, and V_{P_i} can be found as shown in section (4.2.4.b).

At last, the vector of potentials ϕ is obtained by the denormalized inverse transform of V, ie.,

$$\phi = r_e \Psi = r_e T V \tag{4.54}$$

expressing the solutions analytically along the discretization lines in terms of y.

Finally, the following remarks need to be noted:

1. The matrix D in eq. (4.34) applies for Dirichlet-Dirichlet lateral boundaries. However, for the remaining lateral boundary configurations, its form is shown in appendix B.
2. For the case of nonuniform discretization, the eigenvalues and the eigenvectors of the matrix D_{xx} are determined numerically by a suitable procedure such as the "implicit QL-algorithm " [50].

3. It is for the user to select the convenient discretization pattern for his application. However, for uniform error distribution, successive interval sizes should not differ considerably.
4. For $h_i = e_i = h$, r_e and r_h reduce to identity matrices and the analysis simplifies to the one developed for equidistant discretization.

4.4 Conclusion:

Throughout this chapter, it has been shown that the method of lines may be applied for the solution of Poisson's equation for both uniform and nonuniform discretization schemes. It has been also observed that this technique presents interesting features such as simple mathematical formulation, and no primary solution assumption. Furthermore, the analytical form of the solution along the discretization lines, and nonuniform discretization, are aspects that allow to obtain accurate results with less numerical efforts.

To take advantage from these features in semiconductor device modeling, the developed tool is used in the next chapter to provide solutions for practical problems encountered in the determination of the potential distribution within these devices.

Chapter 5

PRACTICAL CONSIDERATIONS

The waveguides that have been investigated using the method of lines consist of multi-layer dielectric materials at the interface of which metallic strips are deposited, and the whole structure is enclosed in a rectangular metallic shielding. However, semiconductor devices may present mixed boundaries due to the external electrode configuration, and special geometry such as MOS structures and curved regions. In this chapter, the previously developed analysis is adapted to these situations.

5.1 Lateral boundaries:

In section (4.2.2), the lateral boundaries are assumed to present zero potential (ϕ) and zero external field component $\left(-\frac{\partial\phi}{\partial x}\right)$ for respectively Dirichlet and Neumann lateral conditions. In this section, general forms of these boundaries are considered.

5.1.1 Generalized Dirichlet condition:

Suppose that there is an electrode on the left side of the structure in fig. (5.1) of a known voltage that we assume to be expressed by:

$$\phi_0 = v(y) \tag{5.1}$$

Inserting this equation in eq. (4.10.a) then the discretized Poisson's equation corresponding to the first line is written as

$$\frac{d^2\phi_1}{dy^2} + \frac{v(y) - 2\phi_1 + \phi_2}{h^2} = f_1 \tag{5.2}$$

Transposing $\frac{v(y)}{h^2}$ to the right side, we get:

$$\frac{d^2\phi_1}{dy^2} + \frac{-2\phi_1 + \phi_2}{h^2} = f_1 - \frac{v(y)}{h^2} = f_1' \tag{5.3}$$

In this equation we note that the second difference operator is identical to the one in eq. (4.11.a). Hence, the same procedure, described in the previous chapter, is carried out with the exception that the element f_1 of the vector f, defined in eq. (4.12.b), is modified as shown in eq. (5.3).

5.1.2 Generalized Neumann condition:

If the external electric field component at the left side of the device takes the form $e(y)$, then this can be approximated by:

$$e(y) = \frac{\phi_1 - \phi_0}{h} \tag{5.4}$$

Combining this equation and eq. (4.10.a), then the discretized Poisson's equation corresponding to the first line becomes:

$$\frac{d^2\phi_1}{dy^2} + \frac{-he(y) - \phi_1 + \phi_2}{h^2} = f_1 \tag{5.5}$$

or equivalently,

$$\frac{d^2\phi_1}{dy^2} + \frac{-\phi_1 + \phi_2}{h^2} = f_1 + \frac{e(y)}{h} = f_1' \tag{5.6}$$

Again, in this case we observe that the second order difference operator is the one in eq. (4.11.b), and the same analysis applies for the remaining steps with the modification, shown in eq. (5.6), concerning the first element of the vector f.

5.2 Horizontal boundaries:

A same semiconductor device surface may include electrodes of known voltages, and free parts on which Neumann condition is assumed. Because of this mixed boundary configuration, special analysis should be carried out. In this example, the voltage profile within the arbitrary two-layer planar structure shown in fig. (5.1) is investigated. To consider the equations describing the conditions at the interface between the layers and to observe the potential behavior at the singularity on the right side of the electrode, the x variable is discretized.

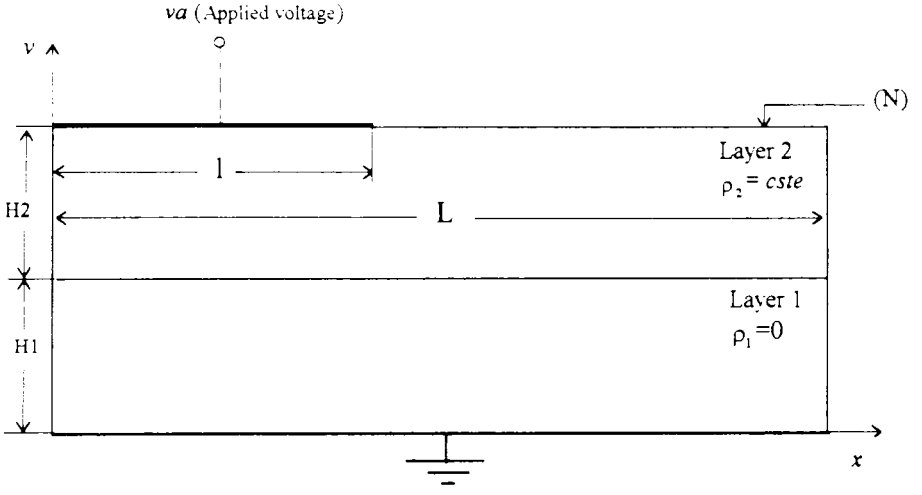

Fig. (5.1) Cross sectional view of the considered structure.

For this purpose, the following equation is considered in both layers

$$\frac{\partial^2\phi(x,y)}{\partial x^2}+\frac{\partial^2\phi(x,y)}{\partial y^2}=-\rho(x,y)\ \varepsilon \tag{5.7}$$

If h is the discretizing interval size, then the total number of lines is given by $N = L\ h$ among which $m = l\ h$ cross the electrode.

Applying the analysis in section (4.2), it can be shown that the transformed solution on the i^{th} line takes the form:

$$V_{1_i}(y) = A_{1_i}\cosh\left(\frac{\chi_i}{h}\right)y + B_{1_i}\sinh\left(\frac{\chi_i}{h}\right)y \tag{5.8.a}$$

in layer 1. However, in layer 2, it is written as:

$$V_{2_i}(y) = A_{2_i}\cosh\left(\frac{\chi_i}{h}\right)y + B_{2_i}\sinh\left(\frac{\chi_i}{h}\right)y + \frac{P_{2_i}}{\varepsilon}\left(\frac{h}{\chi_i}\right)^2 \tag{5.8.b}$$

where the last term represents the particular solution, with P_2 being the transform of the discretized space charge density vector expressed by:

$$P_2 = T^t[1,\ 1,\ldots,\ 1]^t\rho_2 \tag{5.9}$$

For each line, the four constants A_{1_l}, B_{1_l}, A_{2_l} and B_{2_l} should be calculated. For this purpose, a system of four equations describing the potential and displacement vector conditions at the interface between these layers, and the transformed horizontal surface boundaries, must be written by proceeding as follows.

1) Interface conditions:

Interface conditions relate the continuity of the transformed potential and the normal component of the displacement vector $(-\varepsilon dV/dy)$ at the interface $y = H1$, and they are expressed as:

$$V_{1_l}(H1) = V_{2_l}(H1) \tag{5.10}$$

$$\varepsilon_1 \frac{dV_{1_l}}{dy}(H1) = \varepsilon_2 \frac{dV_{2_l}}{dy}(H1) + Qs_l \tag{5.11}$$

where Qs denotes the transform of the eventual surface charge density vector at the considered interface.

2) Surface boundary equations:

These equations are considered on the surfaces $y = 0$ and $y = H1 + H2$, and they are formulated as follows:

a) $y = 0$;

Since the vector of potentials $\phi(0)$ at this surface is zero, then its transform $V(0) = T^t\phi(0)$ is also a zero vector, hence

$$V_{1_l}(0) = 0 \tag{5.12}$$

Consequently, the constants A_{1_l}'s in eq. (5.8.a) ($i=1, \ldots, N$) are zero, and the number of unknowns to find for each line reduces to three.

b) $y = H1 + H2$;

This surface involves an electrode of a length l intersected by m lines on which the condition concerns the potential which takes the value va, and a free surface with a length $(L - l)$ crossed by $(N\text{-}m)$ lines where the normal component of the electric field is zero. Accordingly, the boundary condition on this surface meets one of the following three cases:

***case* 1:** $l = L$ ($m = N$), i.e., Dirichlet condition.

The electrode covers the whole surface and this boundary is described by the *(Nx1)* vector of potentials $\phi = [1,\ 1,\ \ldots,\ 1]^t va$. If we let $Va = T^t\phi$ to be its transform then we have,

$$V_{2_i}(H1+H2) = Va_i \quad ; \quad i=1, \ldots, N. \tag{5.13.a}$$

case 2: $l = 0$ ($m = 0$), i.e., Neumann condition.

There is no electrode and the Neumann condition is assumed on this free surface. Hence, the normal component of the electric field is zero as well as the elements of the transformed electric field vector $(-dV/dy)$. Therefore, we get

$$\frac{dV_{2_i}}{dy}(H1+H2) = 0\ , \quad i=1, \ldots, N. \tag{5.13.b}$$

case 3: $0 < l < L$ ($0 < m < N$), i.e., mixed boundaries.

The boundary condition concerns the potential on m lines and the electric field on the remaining $(N-m)$ ones. Because of the presence of boundaries of different types, neither the transformed vector of potentials nor of electric field can be written on this surface. Hence, this condition can not be formulated in the transformed domain, but it should be considered in the original one, and the procedure to solve the complete problem is summarized as follows:

1. For the i^{th} line, consider the system of three equations (5.10-12) and four unknowns $A_{1_i}, A_{2_i}, B_{1_i}$, and B_{2_i}. in the transformed domain.
2. Solve this system by expressing three unknowns, say A_{1_i}, B_{1_i} and A_{2_i} in terms of B_{2_i}.
3. Rewrite the solutions $V_{1_i}(y)$ and $V_{2_i}(y)$ in eq. (5.8) in terms of B_{2_i}.
4. When achieving the previous steps for $i = 1, 2\ldots, N$, perform the inverse transformation $\phi_2(y) = TV_2(y)$ to express in the original domain the vector of potentials in layer 2.
5. Solve for B_{2_i}'s the system of N equations of the form:

$$\begin{cases} \phi_{2_i}(H1+H2) = va & ; i = 1,\ldots,m. \\ \dfrac{d\phi_{2_i}}{dy}(H1+H2) = 0 & ; i = m-1,\ldots,N. \end{cases} \tag{5.13.c}$$

Remarks:

At this point, the following remarks need to be made:

1. A particular advantage of having a zero potential applied on a given surface (which is usually the case), is that *all the elements* of the transformed vector of potentials take the same value *zero* for this surface. Consequently, the number of unknowns involved in the analytical form of the solution can be reduced by one for all the lines. This is achieved by applying this surface condition just for one line, and the resulting analytical form applies for all the others, as described previously in section (5.2.2.a).
2. It is useful to solve the equations describing the interface and surface conditions in the transformed domain. The reason of this is that N systems of few equations (three in the previous example) are solved separately. However, if the condition concerns the potential for a part of a given surface and the electric field for the other part, then a system of N equations must be considered for this boundary in the original domain, as summarized in case 3 above.
3. In the case where more layers are present then other interface conditions are considered on the additional interfaces.
4. If there are many separate electrodes at $y = H1 + H2$, say two with the voltages va and vb, then the system (5.13.c) is modified accordingly to match the applied voltage on the corresponding lines.

5.3 Geometrical considerations:

5.3.1 Devices having layers of different widths:

Semiconductor structures such as MOS devices may consist of layers of different widths, as illustrated in fig. (5.2).

If h is the discretizing interval size, then $N = L \quad h$ and $M = l \quad h$ are the number of lines crossing respectively the layers (1-2) and 3 ($N \neq M$). As a result, the difference operator sizes and, hence, the eigenvalues and the transformation matrices that apply for layers (1-2) are different from those defined for layer 3. Accordingly, assume T_I^t and T_{II}^t to be the

corresponding transformation matrices, and V_{I1}, V_{I2} and V_{II3} the transformed potential vectors for respectively layer 1, 2 and 3.

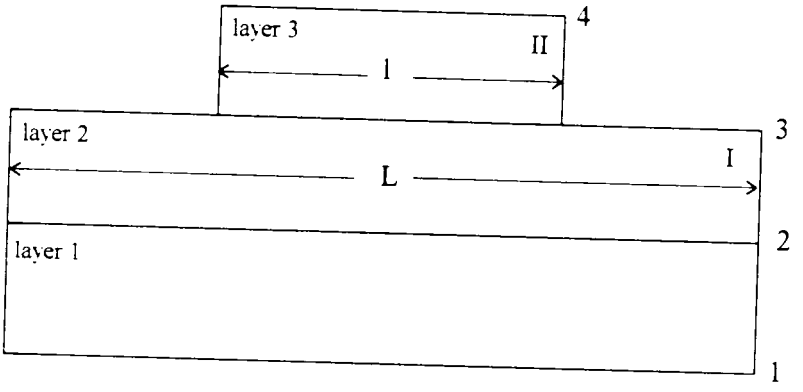

Fig. (5-2) Illustration of a structure with layers having different widths (l < L).

Like in the third case of the previous example, equations describing boundary and interface conditions similar to those in (5.10-12) are first solved separately for layers (1-2) at the surface 1 and interface 2, and for layer 3 at the surface 4. After this step, we will be left with N unknown coefficients related to layers (1-2), and M coefficients related to layer 1, with the condition on the interface 3 not yet considered. After this stage, perform the back transformations:

$$\phi_2 = T_I V_{I2} \tag{5.14.a}$$

and

$$\phi_3 = T_{II} V_{II3} \tag{5.14.b}$$

where $\phi_{2(3)}$ denotes the vector of potentials in layer 2 (3), and then solve in the original domain the system of $(N-M)$ equations consisting of:

- $2M$ equations describing the potential and the displacement vector conditions at the interface between layers 2 and 3, and
- $(N-M)$ equations describing the conditions at the right and left sides of the interface 3.

5.3.2 Curved depletion regions:

It is seen in section (2.3.1.b) that when a semiconductor device is reverse biased, a space charged (depletion) region builds up, with the position of the limits being such that the potential drop within this region is equal to the applied difference of potential. This border may present curved parts and results in curved regions as shown in fig. (5.3) below:

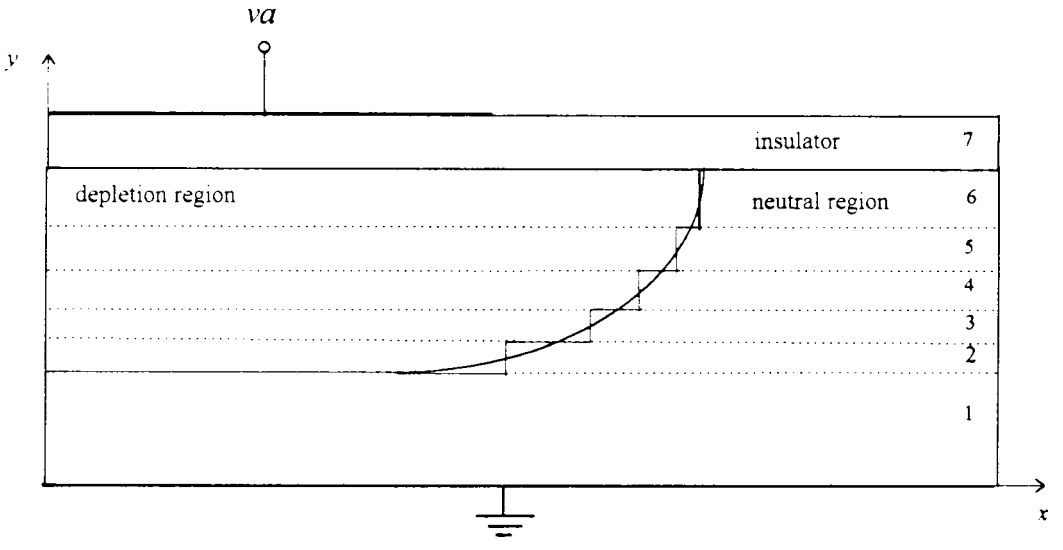

Fig. (5.3) Stair-steps approximation of a curved boundary.

As observed previously, the method of lines is suitable for planar boundaries. A suggestion to overcome the problem of curved limits in semiconductor device modeling is to approximate this border by stair-steps as illustrated in fig. (5.3). As shown in this figure, this is achieved by first subdividing the curved layer into a set of sub-layers (2-6).

We recall that the transformed potential on the i^{th} line and k^{th} layer $(i = 1,\ldots,N\,;\ k = 1,\ldots,7)$ is:

$$V_{k_i}(y) = A_{k_i}\cosh\left(\frac{\chi_i}{h}\right)y + B_{k_i}\sinh\left(\frac{\chi_i}{h}\right) + V_{P\,k_i} \qquad (5.15)$$

where the particular solution V_{p_k} is zero for k = 1 and 7, and depends on the i^{th} element of the transformed space charge density vector obtained for each of the remaining layers $(k = 2, \ldots, 6)$. Accordingly, if $\rho(y)$ denotes the space charge profile, then this vector in the original domain is expressed as:

$$\rho_k = [1,\ldots,1,\ 0,\ldots,0]^t\,\rho(y) \tag{5.16}$$

where the number of non-zero elements is m_k, and this is the number of lines crossing the charged part of the k^{th} layer. Moreover, it can be seen in fig. (5.3) that,

$$m_2 < m_3 < \ldots < m_6 \tag{5.17}$$

Finally, to find the unknown coefficients A_{k_1}'s and B_{k_1}'s, the previously described procedure is carried out with a total number of 7 layers.

5.3.3 Symmetrical structures:

If the geometry and the boundary conditions of a given structure are symmetrical with respect to an axis as illustrated in fig. (5.4), then the potential profile is also symmetrical. Hence, at any two symmetrical points close to that axis, the potential is the same and, therefore, the horizontal electric field component vanishes in there. Consequently, the numerical effort can be reduced significantly by investigating only half of this device, with Neumann lateral condition assumed on the resulting surface.

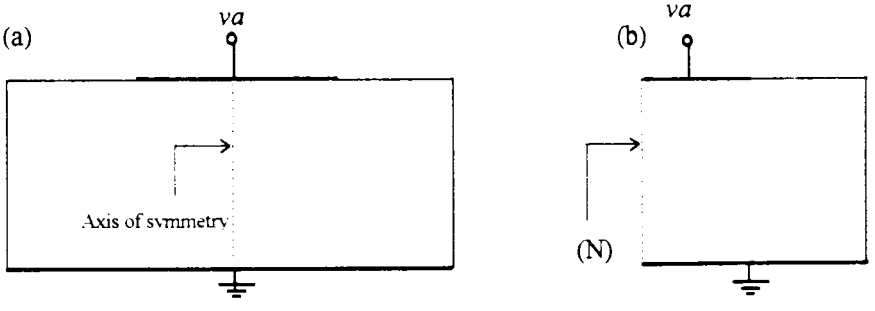

Fig. (5.4) (a) Example of a symmetrical structure, (b) investigated part.

5.4 Conclusion

In this chapter, it has been shown how the developed mathematical tool based on the method of lines can be applied to solve problems related to planar semiconductor devices. Also, it has been proved that the proposed analysis can be extended to include curved boundaries, which makes it is suitable for the analysis of nonplanar structures such as beveled power devices. Furthermore, the presented analysis is flexible to take into consideration the oxide charge and interface state densities that may exit in a MOS structure.

In order to demonstrate the computational power of this technique, some numerical examples are considered in the next chapter and the results are plotted as well.

Chapter 6

NUMERICAL EXAMPLES

A set of computer programs is implemented to demonstrate the efficiency of the analysis described in the two previous chapters. This includes some illustrative examples, which span various possible geometrical and boundary configurations, followed by two practical examples dealing with a *p-n* junction diode and a MOS capacitor in which the depletion layer is delimited and the resulting potential distribution is computed as well.

6.1 Software description:

The programs are written using the MATLAB software package dedicated for scientific and engineering numerical calculations, and can be executed on any of the widely available Personal Computers.

The detailed coding steps involved in the algorithm when using a nonuniform discretization scheme are as follows:

1. - Enter the geometry of the structure and the dimension of each layer as well as the boundary conditions, the charge profile and the discretization scheme.
2. - Perform the discretization by constructing the normalization matrices r_h and r_e, defined earlier in eqs. (4.31) and (4.37).
   - Build the difference operators D_x and D_{xx}, referring successively to eqs. (4.34), (4.40) and (4.41).
3. - Find the eigenvalues of D_{xx}, and build the matrix of eigenvectors, T.
4. - Find the transformed space charge density and surface potential vectors.
5. At this stage the solution can be expressed in the transformed domain by eq. (4.50). To

find the unknown constants A_i's and B_i's for the different layers, proceed as follows:

- Solve the system consisting of the interface conditions (eqs. (5.10-11)) and those describing homogeneous surface boundaries.
- Repeat this operation for all the discretization lines.
- If a surface involves mixed conditions, solve the system (5.13.c) for the remaining unknowns. Similarly, if the device includes layers of different widths, solve the system describing the condition at the interface between these layers, as summarized in section (5.3.1). This case assumes additional discretization scheme and transformation matrix that must be considered in steps (1-3) above.

6. - Perform the inverse transformation (4.54).

If it is desired to evaluate the potential in a given horizontal section or layer, it requires less effort when computing first the solution in the transformed domain and then doing the back transformation, than starting first by transforming the analytical form of the solution to the original domain.

It is important to note that this algorithm applies also for the particular case of uniform discretization. However, for this type of discretization, a much simpler algorithm based on the analysis developed in section (4.2) has been implemented. Besides the specification of the number N of lines in the input stage, the major difference with the previous algorithm concerns mainly steps 2 and 3, which are modified as follows:

2. - Find the discretization interval and build the second order operator P expressed in eq. (4.14).

3. - Find the eigenvalues of the matrix P and form the matrix of the corresponding eigenvectors T, which are expressed analytically in appendix A. Moreover, the back transformation performed in step 6 is the one shown in eq. (4.25).

6.2 Illustrative examples:

The purpose of this part is to verify the applicability of the developed tool, and see how the obtained results fit the prescribed conditions. This consists in finding the potential distribution within arbitrary structures covering a variety of geometrical configurations and boundary conditions.

6.2.1 Boundary condition effects:

In this investigation, a special interest is directed towards the boundary conditions. For this purpose, we propose to find the potential profile in the double layer structure shown in fig. (6.1). This device, having an electrical permittivity constant ε and a constant space charge density ρ, is connected to an electrode on which is applied a dc voltage *Va*. This investigation is carried out through the following four examples.

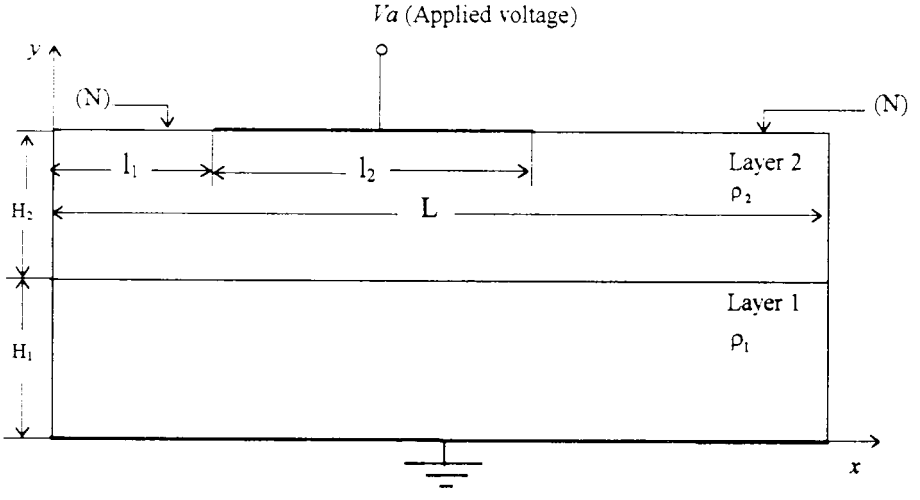

Fig. (6.1) Cross sectional view of the considered structure.
(Refer to dimensions in text)

a) In this example, the potential distribution in the structure is found for different lateral boundary configurations. Accordingly, we let,:

$\rho_1 = 10^{-11}$ C / cm^3; $\rho_2 = -2 \times 10^{-11}$ C / cm^3;

$Va = 20\ V$; $\varepsilon_1 = \varepsilon_2 = 11.9\ \varepsilon_0$; $\left(\varepsilon_0 = 8.85 \times 10^{-12}\ \text{F/m}\right)$.

L = 30 μm; l_1 = 8 μm; l_2 = 10 μm; H_1 = 10 μm; H_2 = 5 μm.

Applying uniform discretization with a discretizing interval size $h = 1\ \mu m$, resulting on a total number of 30 intervals, and assuming successively the lateral conditions:

a) Neumann-Dirichlet, b) Dirichlet-Neumann, c) Dirichlet-Dirichlet, and c) Neumann-Neumann, we obtain the potential contours shown in fig. (6.2).

In these figures (a-d) which represent the device, the curves show equipotential lines with a definition that an equipotential line is a curve joining points of the structure having the same potential. The 7 lines in each of them correspond to potentials varying from 19 Volts near to the electrode, to 1 Volt near to the ground with a step of 3 Volts. Furthermore, the potential at the electrode is found to be Va (20 Volts) and decreases gradually to meet the value zero at the bottom, as fixed by the applied voltages.

Looking separately at these figures, we observe that, near to the lateral boundaries with Dirichlet condition, the potential approaches the value zero. However, at surfaces with Neumann condition, the equipotential lines are normal to these surfaces indicating a zero external field component as specified by this boundary type.

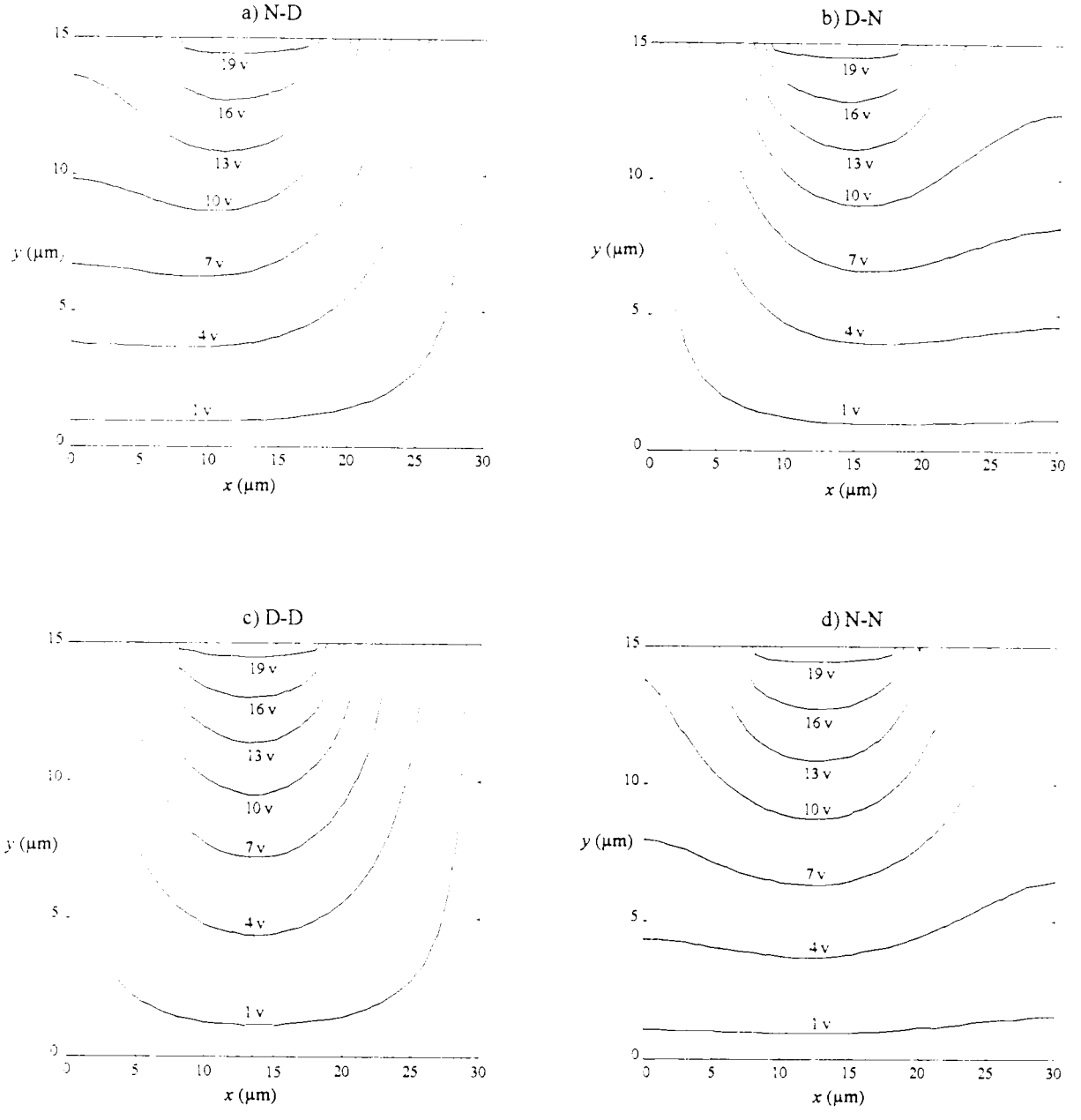

Fig. (6.2) Potential Profiles in the structure in fig. (6.1) with a) Neumann-Dirichlet, b) Dirichlet-Neumann, c) Dirichlet-Dirichlet and, d) Neumann-Neumann lateral boundary conditions.

b) In this example, the previous structure, with the same physical parameters, is considered with Neumann-Dirichlet lateral conditions. However, in this case, the external electric field component strength on the surface with Neumann condition is no more zero, but it is equal to 0 . 5 V / μm.

Introducing the modification expressed in eq. (5.5), we obtain the potential distribution shown in fig. (6.3). Compared to the profile in fig. (6.2.a), we observe in this figure that the lines are bent near the surface with Neumann condition, resulting in a horizontal gradient component which correspond to the electric field intensity specified in this direction.

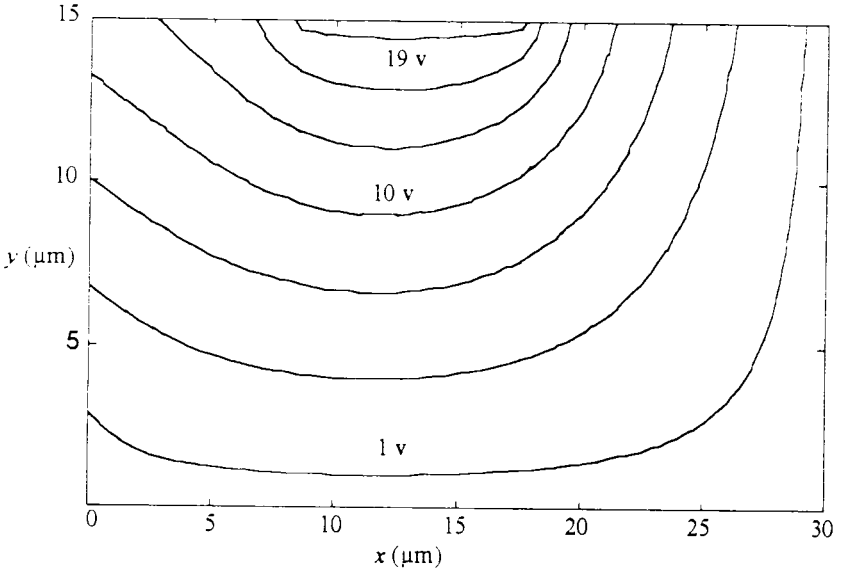

Fig. (6.3) Potential profile in the device in fig. (6.1) with Neumann-Dirichlet boundaries and a left external electric field component different from zero.

c) In this case, the structure in example (a) is still considered with the same physical parameters and dimensions, except that the electrode length is $l_2 = 12$ μm and it is distant from the left corner by $l_1 = 2$ μm.

The purpose of this example is to observe the effect of putting an electrode with a voltage Va ($\neq 0$ Volt) near a surface with Dirichlet condition (0 Volt). Accordingly, we assume Dirichlet-Neumann lateral boundaries, and the resulting potential profile illustrated in fig. (6.4) shows an abrupt potential change on the top left corner of the device, indicating a huge electric field intensity in this area as expected by this boundary configuration.

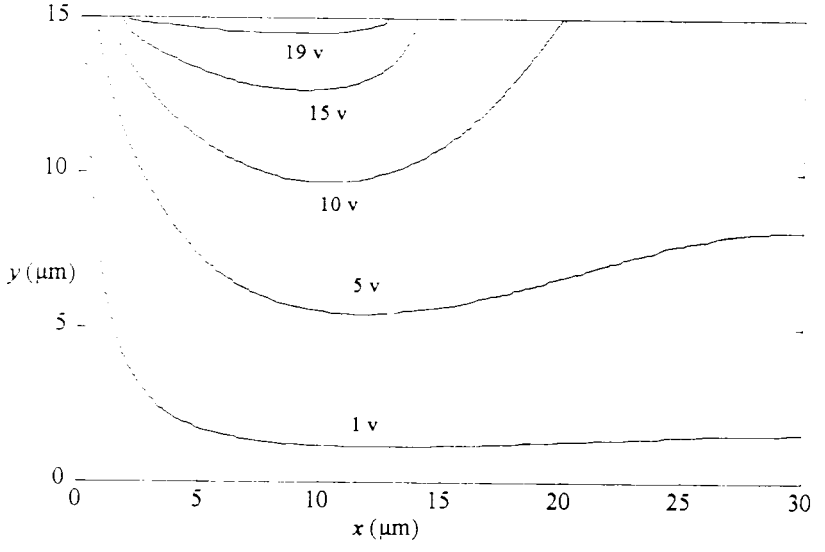

Fig. (6. 4) Potential profile in the structure in fig. (6.1) with l_1 =2 μm and Dirichlet-Neumann lateral boundaries.

d) In this example, Neumann-Neumann lateral boundary set up is assumed for the device in example (a) with $l_1 = 0$ μm. Four different voltages (5, 10, 15, and 20 Volts) are successively applied at the electrode, and the resulting potential distributions at the top surface $(y = H_1 + H_2)$, shown in fig. (6.4), indicate an important potential variation around the electrode edge. Consequently, a nonuniform discretization scheme, with discretizing intervals smaller around the electrode edge and greater elsewhere, is convenient for better accuracy with no extra numerical effort as demonstrated in the next section.

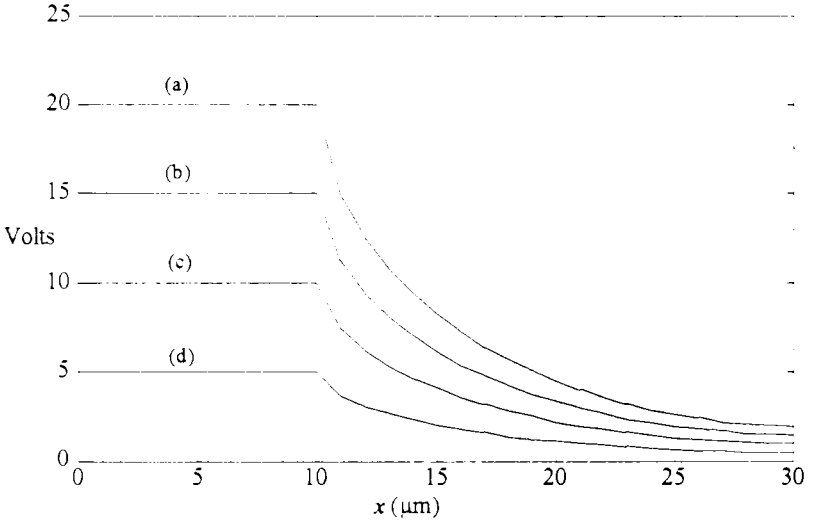

Fig. (6.5) Surface potential distribution on the structure in fig. (6.1) with: l_1=0, l_2=10 μm, Neumann-Neumann lateral boundaries, and the electrode voltages: (a) 20, (b) 15, (c) 10 and, (d) 5 Volts.

6.2.2 Nonuniform discretization:

In this section, nonuniform discretization is introduced and applied for the structure of the previous example, with: $H_1 = 5.0$ μm, $H_2 = 2.5$ μm, $Va = 10\ V$ and Neumann-Dirichlet lateral conditions. In this investigation, we are interested by the potential distribution at the interface between the two layers (y=H_1).

First, uniform discretization is performed and the obtained results shown in fig. (6.6) indicate that, with increasing number of discretization lines N, there is a rapid convergence towards a given potential distribution. Similarly, it has been seen in microwave device

analysis that, when a specific parameter is investigated using this method, the solution converges always smoothly, and the 'exact' value can be determined by means of extrapolation when the discretizing interval approaches zero [29].

Furthermore, we observe in this figure a rapid potential variation around the electrode edge (x = 10 μm), and it is almost constant and linear respectively on the left and the right parts of the devices where accurate results are already obtained with 12 lines, and no substantial improvement is provided by extra lines as predicted by eq. (4.7) in which the error terms vanish for constant and linear profiles.

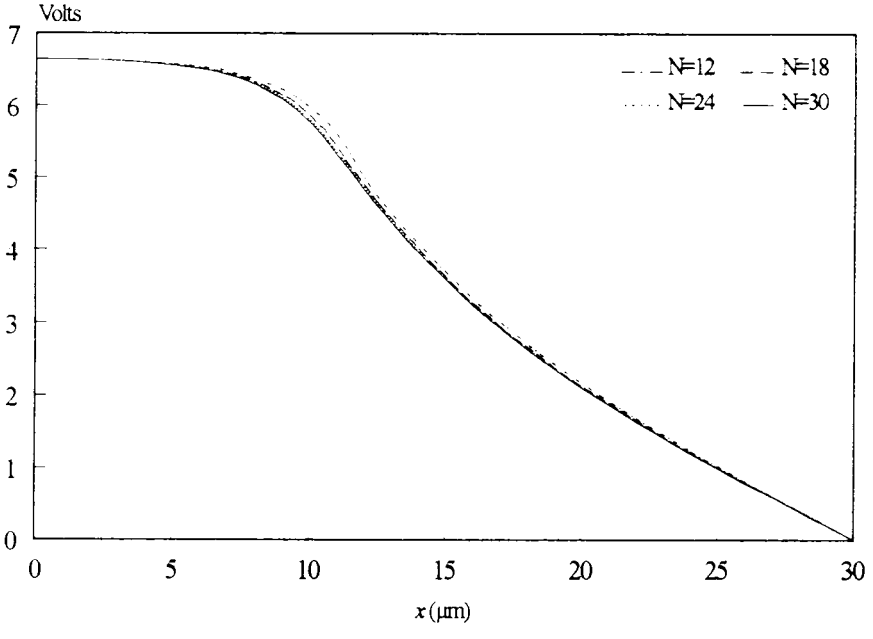

Fig. (6.6) Convergence behavior of the method of lines seen on the potential distribution at the horizontal surface y=H1, with H1=5 μm, H2= 2.5 μm and Va=10 Volts.

Accordingly, a nonuniform discretization pattern produced by 13 lines with small intervals around the electrode edge and greater elsewhere, as illustrated by the horizontal dot spacing in fig. (6.7), is performed. We observe in this figure that these dots, which show also the results obtained from this pattern, lie on the continuous curve corresponding to the distribution resulting from 30 uniformly spaced lines, providing similar accuracy with significantly small number of lines.

In addition to accuracy improvement, this type of discretization reduces significantly the computational effort, since the size of matrices that are put into use by the algorithm and the required computation time depend strongly on the total number of lines.

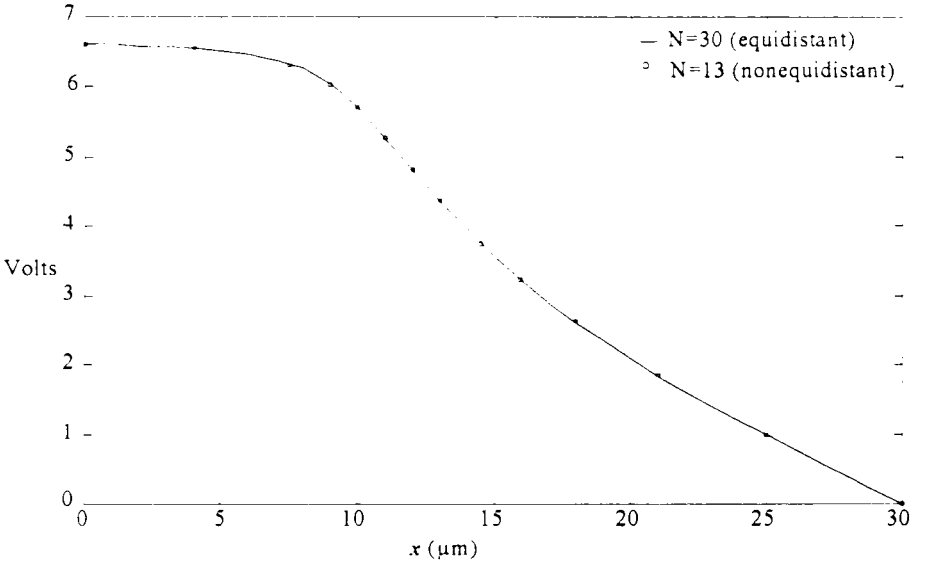

Fig. (6.7) Illustration of the convergence behavior of nonequidistant discretization applied for the structure of the previous example.

6.2.3 Symmetrical structures:

In this example, the two-layer symmetrical structures shown in fig. (6.8) are considered, and the results compared with those obtained when halves of these devices are investigated. In both structures, the layer near to the ground has a constant charge density ρ_1, whereas the charge profile in the second layer is linear of the form $\rho_2 = A(y - H_1) + B$.

- The common dimensions and physical parameters for both structures are:

  $\rho_1 = 3.5 \times 10^{-11}\ C/cm^3$; $A = -10^{-13}\ C/cm^4$; $B = -10^{-11}\ C/cm^3$; $\varepsilon = 11.9\ \varepsilon_0$;

  $L = 30\ \mu m$; $H_1 = 2.5\ \mu m$; $H_2 = 15\ \mu m$; $Va = 20\ V$.

- Specific parameters for the structure in (a):

  $l_1 = l_2 = 10\ \mu m$; Lateral conditions: Dirichlet-Dirichlet.

- Specific parameters for the device in (b):

  $l_1 = l_2 = 6$ μm; Lateral conditions: Neumann-Neumann.

The analysis is carried out with a total number of 63 uniform intervals for the device in (a) and 65 for the device in (b). It can be seen from fig. (6.9) that the obtained potential profiles are similar when the complete structures and the right parts, with Neumann condition at the symmetry axes, are investigated separately. Moreover, it is verified that the *'analytical'* results are identical for symmetrical lines when the whole device is investigated, and they are equal to those obtained when only half of the structure is investigated. Consequently, for such devices the numerical effort can be reduced significantly by reducing the total number of lines by a factor of two.

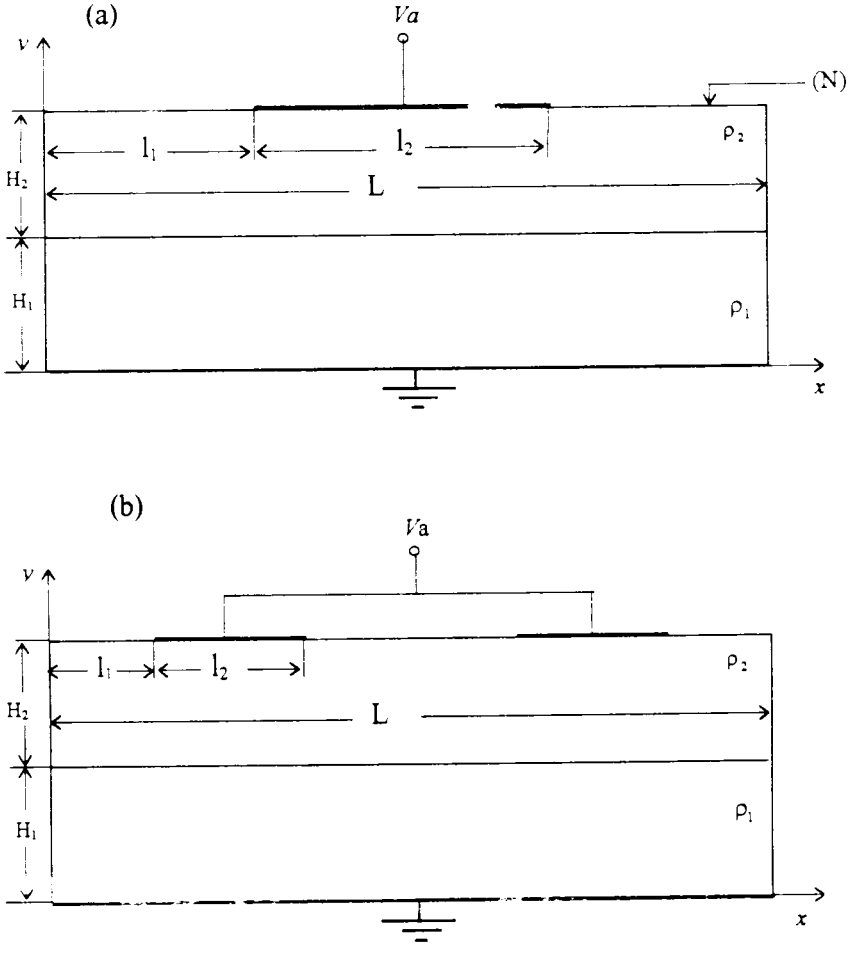

Fig. (6.8) Cross sectional view of the assumed symmetrical structures. (Refer to dimensions in text).

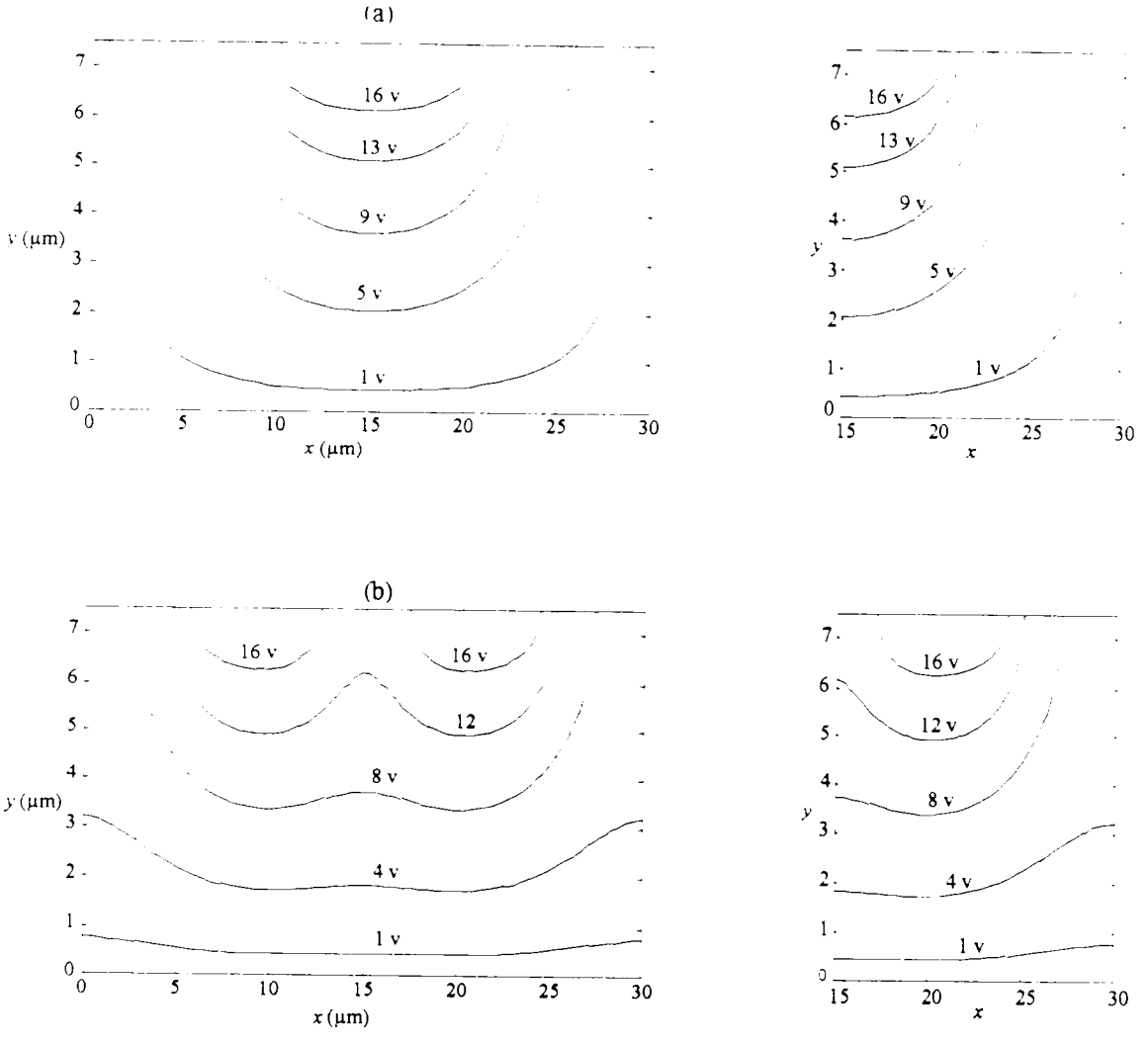

Fig. (6.9) Potential Profiles throughout the whole and right parts of the symmetrical structures in fig. (6.8), when investigated separately.

6.2.4 Structures with layers of different widths:

It is shown in section (5.3.1) that devices including layers having widths of different size such as MOS devices, need a special mathematical handling of the interface conditions between these layers which should be expressed in the original domain.

A typical shape of such devices is the three-layer structure shown in fig. (6.10) for which we propose to find the potential distribution. For this purpose, we assume the charge density

profiles to be a constant ρ_1 in layer 1, exponential of the form $\rho_2 = Ae^{\alpha(y-H_1-H_2)} + B$ in layer 2, and zero in layer 3. Accordingly, we let

$\rho_1 = 10^{-11}\ C\ \ cm^3$

$A = -10^{-11}\ C\ \ cm^3$; $B = -5 \times 10^{-14}\ C/cm^3$; $\alpha = 10^8\ \ cm$

$Va_1 = 4\ V$; $Va_2 = 14\ V$; $Va_3 = 8\ V$.

$\varepsilon_1 = \varepsilon_2 = 11.9\ \varepsilon_0$; $\varepsilon_3 = 3.9\ \varepsilon_0$; $l_1 = l_2 = l_3 = 10\ \mu m$.

$H_1 = 10\ \mu m$; $H_2 = H_3 = 5\ \mu m$.

Lateral boundaries: Neumann-Neumann for the layers (1-2) and 3.

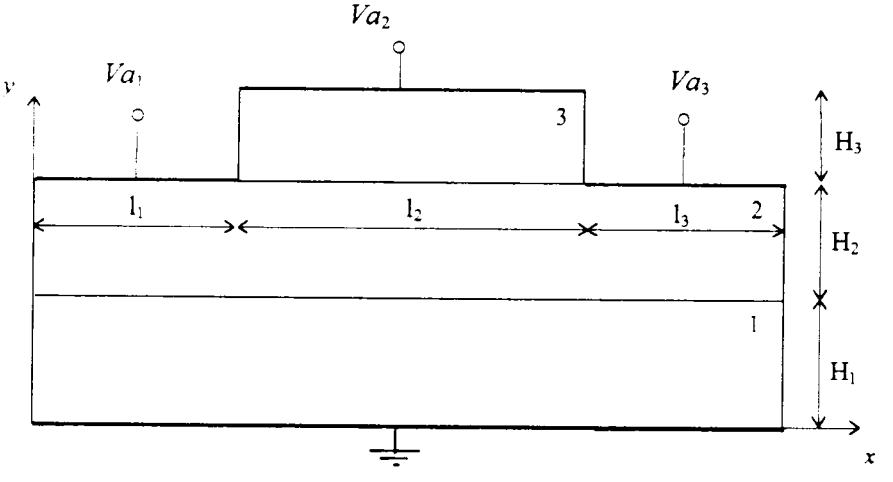

Fig. (6.10) Considered structure of width sizes $l_1 + l_2 + l_3$ for layers (1 and 2), and l_2 for layer (3).

A uniform discretization with a total number of 36 lines in layers 1 and 2 and 12 in layer 3 has been performed, and the obtained profile is shown in the three-dimensional plot in fig. (6.11). In this figure, the horizontal plane represents the device geometry and the heights where the mesh nodes are located indicate the potential strength at the corresponding points. As set by the boundary condition, we observe in this figure that the potential increases from the grounded surface on the bottom of the structure to the applied voltages at the respective electrodes. Further, near to the lateral surface of the device there is no lateral potential variation and this agrees with the Neumann condition assumed on these edges. Moreover,

we observe that the potential rate of change in the y direction, which reflects the vertical electric field component, presents a discontinuity at the interface between layers 2 and 3, caused by the difference in electrical permittivity between the two media as predicted by the interface condition in eq. (2.23).

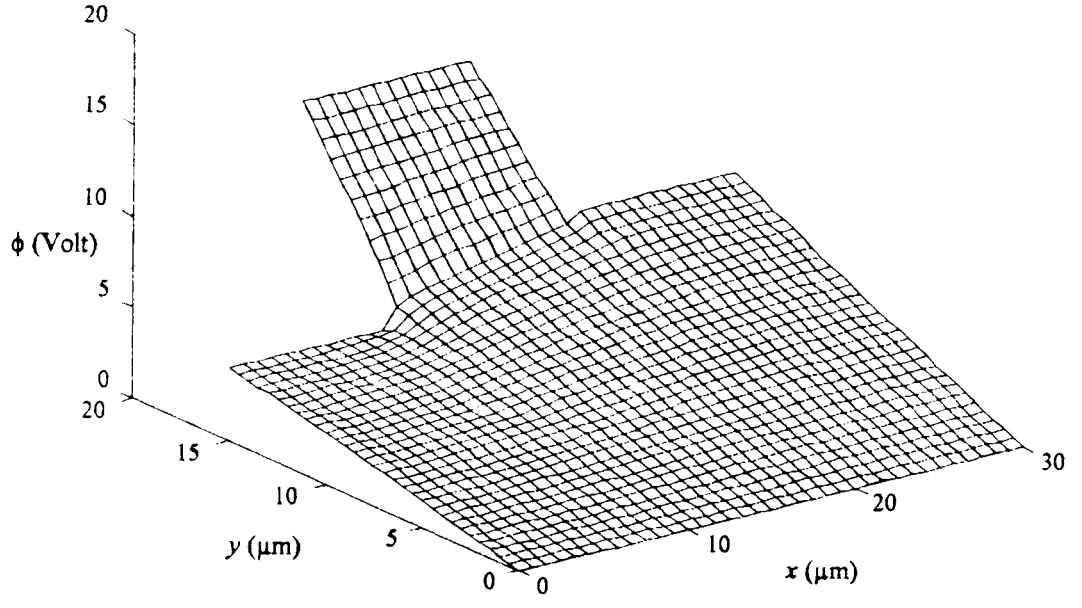

Fig. (6.11) Three-dimensional potential representation in the structure of fig. (6.10).

6.3 Semiconductor devices analysis:

In this section, semiconductor device analysis is carried out. This involves one dimensional investigation of a *p-n* junction and a two-dimensional analysis of a MOS capacitor.

6.3.1 One-dimensional *p-n* junction analysis:

In section (2.1), a closed form analytical solution is obtained for the one-dimensional Poisson's equation, and materials related to reverse biased *p-n* junction are provided. In this section, the developed semianalytical tool is applied to a similar device, shown in fig. (6.12), with boundary assumptions producing a one-dimensional profile.

Indeed, a one dimensional analytical solution can be easily obtained for this example, however, the objective of this analysis is to test how the results obtained with this seminumerical scheme fit the analytical ones.

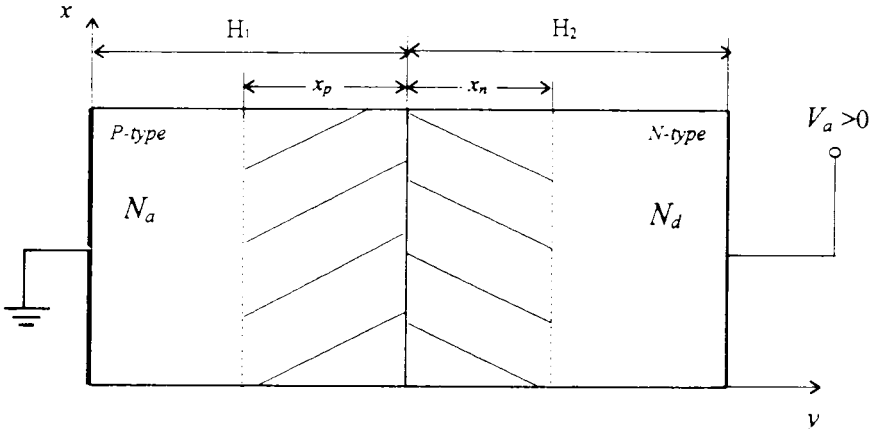

Fig. (6.12) Reverse-biased *p-n* junction physical model.

One dimensional profile assumption for this example supposes infinite device width and no field component along *y*-direction, and this is translated by Neumann-Neumann lateral boundaries when using a two-dimensional tool.

The investigation is carried out under these conditions with the depletion layer widths expressed by eqs. (3.9), and it can be seen in fig. (6.13) that the obtained profile is in fact one dimensional since the contour lines are horizontal, verifies the equilibrium conditions and is similar to the one obtained analytically in section (3.1).

Mathematically, the agreement between these results and the analytical ones is explained by the fact that, with Neumann-Neumann lateral boundaries, one eigenvalue of the second order operator is zero, and the solution of the corresponding ordinary differential equation in (4.21) is a second degree polynomial. Furthermore, it has been observed that the contribution of the other eigenvalues (terms in *sinh* and *cosh*) is zero. Accordingly, the profile in the original domain is also parabolic and, consequently, the one-dimensional

possible analytical solution for this problem is revealed and provided by this semianalytical technique.

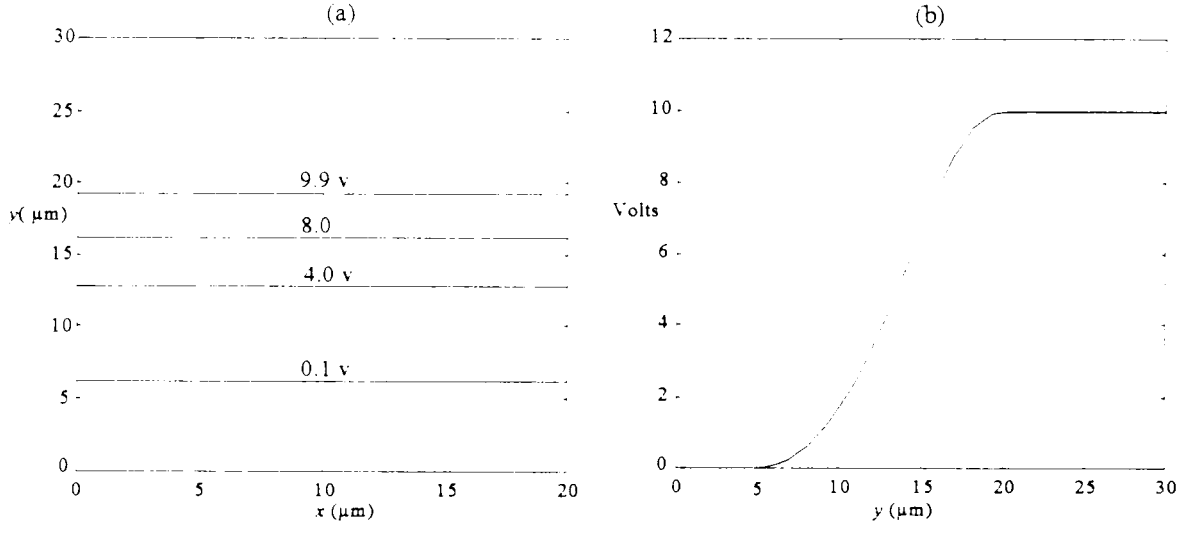

Fig. (6.13) Potential profile in the silicon diode of fig. (6.12) with $N_d=2N_a=1.7\ 10^{14}\ /\ cm^3$, $H_1 = H_2 = 15\ \mu m$ and $V_a = 10\ V$. (a) Two dimensional representation and , (b) one-dimensional distribution along y direction.

6.3.2 MOS structure description:

A MOS structure which is the basis of MOS devices consists of a metallic gate, a *P* or *N*-type silicon substrate and an oxide film as shown in fig. (6.14) [51]. Because of the presence of a dielectric material (SiO_2) between the gate and the substrate, this device exhibits the properties of a capacitor which constitutes the basic element of a charge coupled device (CCD's) [52]. The analysis of this device under various conditions is a powerful tool to investigate the quality of the oxide and the oxide-silicon interface [53].

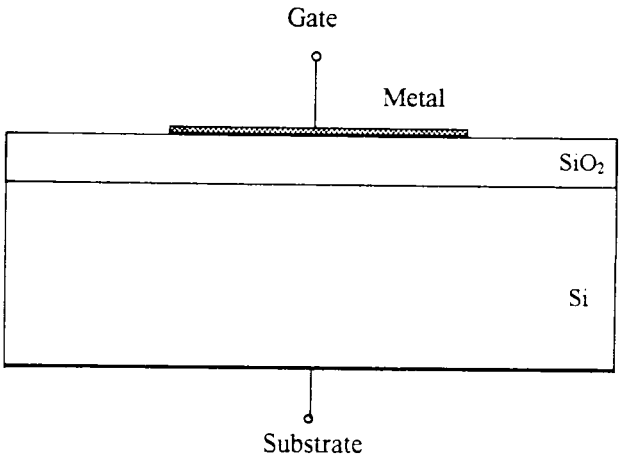

Fig. (6.14) Cross-sectional view of a MOS structure.

In this analysis, it is assumed that the metal and the semiconductor work functions are equal, and there is no charge in the oxide and at the oxide-silicon interface. Under these conditions, the electric field is zero everywhere at zero applied bias [54].

6.3.3 MOS device operating modes:

Under varying gate voltage, a MOS device shows four different modes which are:

1) accumulation, 2) depletion, 3) inversion and, 4) deep depletion.

6.3.3.1 Accumulation mode:

In this mode, the device is biased in such a way the majority carriers are attracted towards the gate. Thus, for a *P*-type silicon when a negative gate voltage is applied, the negative charges on the gate attract holes to the oxide-silicon interface to build up an accumulation layer. The condition of neutrality is satisfied when the charge generated in the metal is equal but of opposite sign to that present in the silicon.

6.3.3.2 Depletion mode:

In the depletion mode, the MOS device is biased in such a way the majority carriers are repelled away from the SiO_2-Si interface towards the bulk. Therefore, for a *P*-type silicon, a positive gate voltage generates a negatively charged layer in the silicon near the SiO_2-Si

interface because the holes repelled by the electric field leave behind the fixed negatively ionized acceptor atoms. The electric equilibrium requires that the potential drop across the oxide and the depletion layer is equal to the gate voltage.

6.3.3.3 Inversion mode:

With increasingly positive applied voltage, the depletion layers continues to widen until electrons (minority carriers) attracted from the substrate appear at the silicon surface in great number an build up a thin inversion layer. The formation of this layer is a threshold phenomenon and occurs when the minority carriers concentration is equal to the doping concentration.

6.3.3.4 Deep depletion mode:

If the gate voltage is increased rapidly starting from a condition of accumulation, there may be not enough time for the inversion layer to form, which is rather a slow process. In this case, the depletion region is set up immediately with a thickness much greater than in inversion mode [54]. This mode, which is a continuation of the normal depletion mode, is considered in the investigation of breakdown phenomenon since it is in this condition that this effect occurs usually [55].

6.3.4 MOS capacitor analysis:

The following analysis consists in finding the space charge limits and the potential profile in a *P*-type MOS capacitor in deep depletion mode, which are major steps in finding the breakdown voltage [55, 56] and the depletion capacitance of such devices [53].

The two-dimensional model of the considered device is assumed to be symmetrical and hence the investigation can be limited to the left part illustrated in fig. (6.15). When a positive voltage is applied at the electrode, free majority carriers (holes) are repelled by the induced electric field. Equilibrium condition requires that the potential is zero at the self adjusting boundaries of the resulting fully depleted layer and elsewhere in the neutral region as explained in section (2.3.1.b).

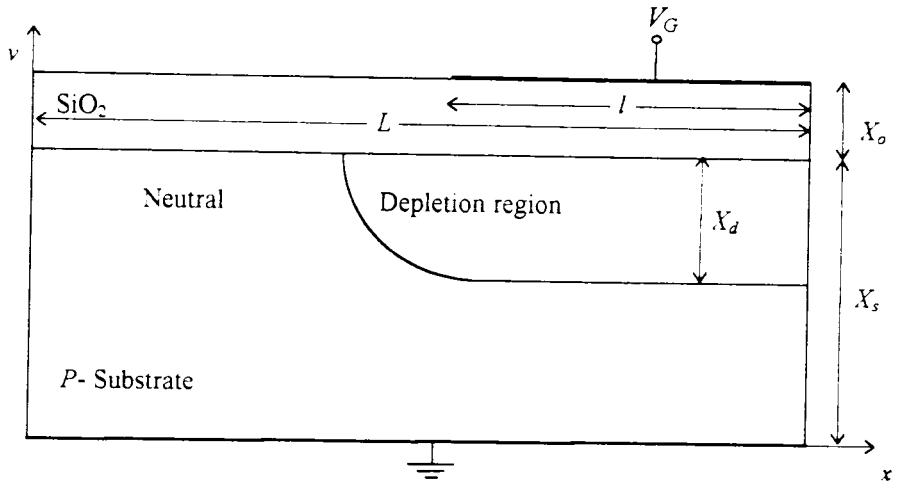

Fig. (6.15) Two-dimensional model of the MOS capacitor used in the present analysis.

We recall that that electric potential distribution is calculated by solving the Laplace's equation:

$$\nabla^2\phi = 0 \tag{6.1}$$

in the oxide and the neutral regions, and the Poisson's equation:

$$\nabla^2\phi = \frac{qN_A}{\varepsilon_s\varepsilon_0} \tag{6.2}$$

in the depletion region, where ε_s and N_A denote respectively the relative permittivity of silicon and the substrate majority carriers density. The lateral boundary conditions of the silicon and oxide layers are of Neumann type.

A similar structure has been considered by Rusu et al in [56] for breakdown voltage investigation. They used finite difference method for the potential profile, and they assumed a rectangular geometry of the space charge region at the central area of the device with a thickness X_d given by the one-dimensional solution of Poisson equation which is

$$X_d = -\frac{\varepsilon_s}{\varepsilon_{ox}}X_o + \sqrt{\left(\frac{\varepsilon_s}{\varepsilon_{ox}}X_o\right)^2 + \frac{2\varepsilon_s\varepsilon_o V_G}{qN_A}} \tag{6.3}$$

and the curved border is supposed to be circular with a radius of the same value X_d.

The discretization pattern involves 10 concentrated equidistant lines crossing the curved area and 31 largely spaced elsewhere. The space charge layer is subdivided into 10 sub-layers to perform stair-steps approximation on the curved boundary as shown in fig. (5.3).

The main steps involved in the algorithm are:

1. - Enter the geometrical and physical parameters as well as the discretization scheme.
2. - Find the eigenvalues and eigenvectors of the second order difference operator.
   - Assume initial depletion layer thickness ($\geq X_d$ in eq. (6.3))
3. - Find the transformed space charge density vectors for the sub-layers.
4. - Find the potential semianalytical expression under this condition.
5. - Check whether the potential satisfies the previously stated condition on the assumed border and neutral region. If it is not fulfilled, readjust the depletion layer border position, and redo step 4. Since the electrode voltage is positive, then the depletion layer width should be increased if the potential on the assumed limit is positive, and decreased if it is negative, until the required condition is satisfied.

The space charge region geometry, assumed in [56] with initial thickness given by eq. (6.3), has been reconsidered in this analysis, besides the following parameters:

$L = 35\ \mu m$; $l = 17\ \mu m$; $0.1 < X_o < 5.0\ \mu m$; $30 < X_s < 50\ \mu m$.

$10^{14} < N_A < 10^{18}\ cm^{-3}$; $10 < V_G < 100\ V$ ($V_G <$ $V_{breakdown}$ reported in [56]).

After executing the program for different X_o and N_A, the following features have been observed:

1) At low oxide thickness and high doping concentration ($X_o < 3\ \mu m$ and $N_A > 10^{15}\ cm^{-3}$), the potential drop in the assumed curved part of the space charge region is excessive, and gets largely negative in this area and in the assumed neutral region, violating the equilibrium condition. Hence, the circular contour assumption of the depletion region is inadequate.

2) At high oxide thickness and low doping concentration, the lateral depletion region border approximation by a circular geometry is convenient. However, in the central area of the

device the initial width X_d needs to be slightly readjusted by a correction factor cf within the range [0.988 - 0.999].

The former remarks are explained by the fact that, for high doping concentrations and low oxide thickness, the depletion region is thin and located closer to the gate. Hence, the electric field becomes predominantly one-dimensional with a small deviation, in the curved area of the depletion region, which is not sufficient to result in a circular border of this layer. However, in case (2), the space charge layer is thicker and located far from the gate. Consequently, the electric field lines deviation in these regions is sufficiently large to induce a circular geometry of the left depletion region border.

Finally, the obtained results for $N_A = 10^{15}\ cm^{-3}$, $X_o = 5.0\ \mu m$ (case 2), $X_s = 30\ \mu m$ and $V_G = 100\ V$, are illustrated in fig. (6.16).

In figure (a) which shows the potential distribution on the right side of the device along the y direction, it can be seen that the profile is linear in the oxide region, parabolic in the depletion layer and zero in the neutral region, as it would be given by the one-dimensional analytical solution. An overview of the profile is illustrated by the three-dimensional plot of the figure in (b). This figure shows a good agreement with the previously stated boundaries and physical requirements with an acceptable error range (0.4 V) corresponding to the maximum potential deviation from zero recorded at the assumed depletion layer border, and this error is smaller elsewhere in the neutral region as s shown by the flat potential profile in there. The former deviation results mainly from the stair-steps approximation of the space charge border, and depends on the discretization pattern, the number of sub-layers defined in this region, and the curved border contour assumption which is not exactly circular but still needs some readjustments. Also, it is important to note that, for these figures, only a part of the sufficiently large neutral region is shown in the y direction.

An important observation is that much numerical effort can still be saved by considering only a part of the neutral region since the potential therein is zero. This last point is particularly important when the left lateral side is far from the space charge region, and consequently, the number of discretization lines can also be reduced.

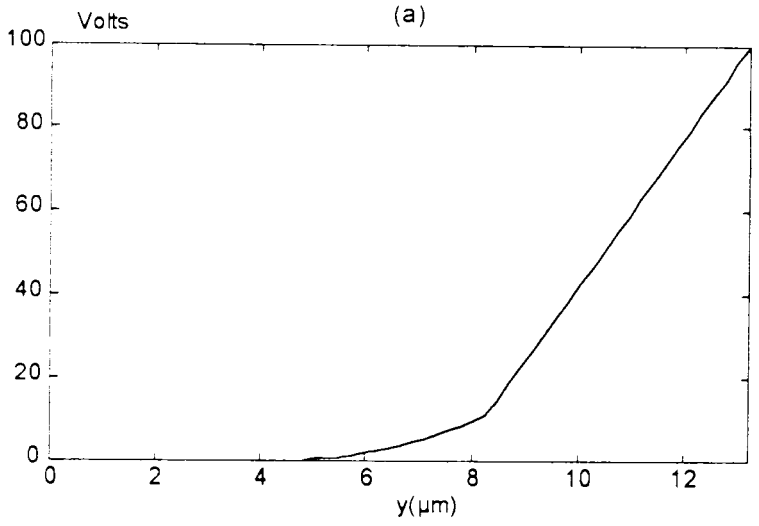

(b)

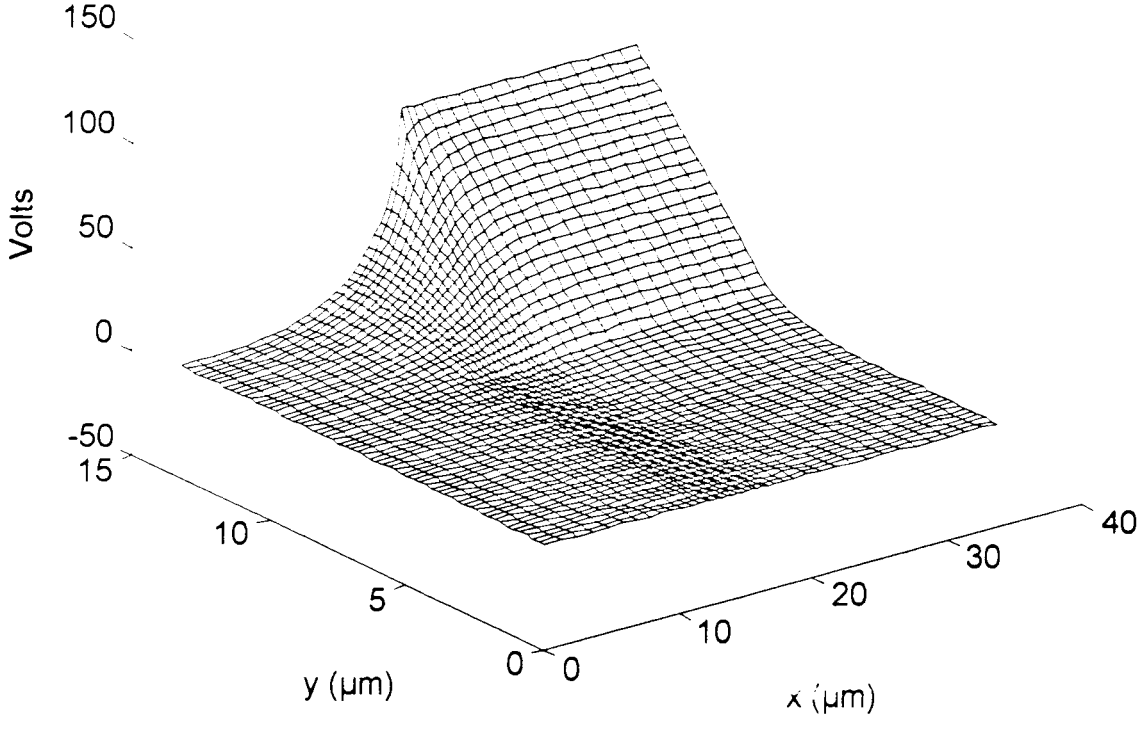

Fig. (6.16). Potential distribution in the device of fig. (6.14), (a) one dimensional profile on the right edge, and (b) three-dimensional representation.

6.4 Conclusion:

In this chapter, it has been observed that the results obtained with the method of lines map with those predicted by the boundary conditions. Further, some important features of this technique which help to save execution time and memory space have been verified. Among these features we note those relative to symmetrical structures and nonequidistant discretization which improve significantly the convergence behavior of this technique.

However, it is observed that, as the ratio between the largest layer thickness and the smallest discretization interval gets high, the systems which should be solved for the coefficients involved in the transformed semianalytical solution might be ill-conditioned. This is due to the fact that terms in *tanh(x)*, where x depends on this ratio, are set to unity as x becomes high. This problem can be overcome by reducing the software precision number and/or subdividing thick layers into sub-layers. Actually, in the analysis of a MOS devices, this problem might be already eliminated when considering only a part the neutral region which is usually the largest one, and when subdividing the space charge layer into thin sub-layers to approximate curved boundaries by stair-steps.

Chapter 7

CONCLUSION

In this work, a semianalytical solution for the two-dimensional Poisson's equation is obtained using the Method of Lines for both equidistant and nonequidistant discretization schemes. The developed mathematical tool is then adapted for practical semiconductor device configurations to provide solutions for space charge limits and potential profiles within these devices. This concerns mainly:

- Structures with generalized Dirichlet and Neumann lateral boundaries with respectively non-zero potential and non-zero external field component.
- Devices with mixed surface boundaries, where the potential is specified only on some parts of the surface, whereas the remaining parts are left free and Neumann conditions have been assumed.
- Structures involving layers of different widths where the continuity conditions at the interface between these layers require special handling.
- Devices with curved boundaries approximated in this work by stair-steps to extend the application of the Method of Lines for nonplanar structures.

Based on these considerations, software programs have been implemented and tested on various configurations. Also, a case study for an actual MOS capacitor has been carried out, and the results map with the expected data.

In addition to the advantages that characterize other techniques used for semiconductor device modeling such as finite difference and finite element methods, this technique is characterized by a set of other features, such as:

- Simplicity in concept and coding.

- High accuracy with less numerical effort.
- No problems of relative convergence. In contrast, there is a monotonous convergence to the exact value when decreasing the discretization step.
- No need for initial guess, and no physically meaningless solutions.

Furthermore, compared to other purely numerical techniques, this method saves considerable amount of time and memory space. Also, once the solution is obtained for a given structure, it can be saved in its analytical form, and its evaluation can be limited to the area of interest within the device.

The application field of the proposed scheme covers the evaluation of depletion capacitance and breakdown voltages for semiconductor devices. This allows mainly, to make optimum designs for specified breakdown voltages, in particular for power devices.

We believe that this work opens a wide research field, and may be subject to more improvements such as:

- Implementation of a compact software package dedicated for the previously indicated applications.
- Extension of the analysis to solve the three-dimensional Poisson's equation to meet current trends in micro electronics technology.
- Consider the complete set of semiconductor device equations, and solve them using this method in conjunction with a variational technique for low and high injection levels.

Finally, we hope that this method which is introduced among the numerical techniques used for semiconductor device analysis provides useful material and constitutes an adequate choice for the stated applications.

APPENDIX A

Eigenvalues and Eingenvectors of the Second Order Difference Operator, *P*.

For equidistant discretization, the second order difference operator is the tridiagonal *NxN* matrix *P* of the form:

$$P = \begin{bmatrix} p_1 & 1 & & & \\ 1 & -2 & 1 & & \\ & 1 & \ddots & \ddots & \\ & & \ddots & -2 & 1 \\ & & & 1 & p_2 \end{bmatrix} \qquad \text{(A.1)}$$

in which p_1 and p_2 depend respectively on the left (right) boundaries, i.e.,

$$p_{1(2)} = \begin{cases} -2 & \text{for Dirichlet condition} \\ -1 & \text{for Neumann condition} \end{cases} \qquad \text{(A.2)}$$

If λ_k is the k^{th} eigenvalue and t_k the corresponding eigenvector, then

$$(P - \lambda_k)t_k = 0 \qquad \text{(A.3)}$$

For the matrix *P* above, this system can be solved analytically [29], and the resulting eigenvalues and the elements T_{ik} of the matrix of eigenvectors are shown below:

Left-Right boundaries	$-\lambda_i$	T_{ik}
Dirichlet-Dirichlet	$4\,sin^2\dfrac{i\pi}{2(N+1)}$	$\sqrt{\dfrac{2}{N+1}}\,sin\dfrac{ik\pi}{N+1}$
Dirichlet-Neumann	$4\,sin^2\dfrac{i\pi}{2N+1}$	$\sqrt{\dfrac{2}{N+1/2}}\,sin\dfrac{i(k-1/2)\pi}{N+1/2}$
Neumann-Dirichlet	$4\,sin^2\dfrac{(i-1/2)\pi}{2N+1}$	$\sqrt{\dfrac{2}{N+1/2}}\,cos\dfrac{(i-1/2)(k-1/2)\pi}{N+1/2}$
Neumann-Neumann	$4\,sin^2\dfrac{(i-1)\pi}{2N}$	$\dfrac{1}{\sqrt{N}}$ *if* $k=1$ $\sqrt{\dfrac{2}{N}}\,cos\dfrac{(i-1/2)(k-1)\pi}{N}$ *for* $k>1$

APPENDIX B

First Order Difference Operators for Nonequidistant Discretization

The form of the first order difference operator D introduced in section (4.3.2) depends on the lateral boundaries. Accordingly, for Dirichlet-Dirichlet it is given by the $(N-1)$xN matrix:

$$D_{DD} = \begin{bmatrix} 1 & & & \\ -1 & 1 & & \\ & -1 & \ddots & \\ & & \ddots & 1 \\ & & & -1 \end{bmatrix} \qquad \text{(B.1)}$$

and for Dirichlet-Neumann, it is expressed by the NxN matrix:

$$D_{DN} = \begin{bmatrix} 1 & & & & \\ -1 & 1 & & & \\ & -1 & \ddots & & \\ & & \ddots & 1 & \\ & & & -1 & 1 \end{bmatrix} \qquad \text{(B.2)}$$

For the remaining Neumann-Dirichlet and Neumann-Neumann configurations, this opearator is identified to be respectively,

$$D_{ND} = -D_{DN}^{t} \qquad \text{(B.3)}$$

and,

$$D_{NN} = -D_{DD}^{t} \qquad \text{(B.4)}$$

REFERENCES

[1] W. Shockley, *"A Unipolar 'Field Effect' Transistor"*, Proc. IRE, pp.1365-1377, November 1952.

[2] A.B. Grebene and S.K Ghandi, *"General Theory for pinched operation of the junction-gate FET"*, Solid State Electron, No.12, p.537, 1969.

[3] M. Shur and L. Eastman, *"Current-Voltage characteristics, small signal parameters, and switching times of GaAs FET's "*, IEEE trans. Electron Devices, ED-25, No.6, pp.606-611, 1978.

[4] H.K, Gummel, *" A self-consistent iterative scheme for one-dimensional steady-state transistor calculations "*. IEEE Trans. Electron Devices, ED-13, pp.4-21, 1966.

[5] A. De Mari, *"An accurate numerical steady-state one-dimensional solution of the p-n junction"*, Solid State Electron, Vol.11, pp.33-58, 1968.

[6] D.P. Kennedy and R.R O'Brien, *"Computer-aided two-dimensional analysis of the junction field-effect transistor"*, IBM J. Res. Dev., Vol.14, pp.95-116, 1970.

[7] J.W. Slotboom, *"Computer-aided two-dimensional analysis of bipolar transistors"*, IEEE Trans. Electron Devices, ED-20, No.8, pp.669-679, 1973.

[8] D.P. Kennedy and R.R. O'Brien, *"Two-dimensional analysis JFET structure containing a conductivity substrate"*. Electron. Lett., Vol. 7, No.24, pp.714-717, 1971.

[9] T. Toyabe, K. Yamaguchi and S. Asai, *"A numerical model of avalanche breakdown in MOSFET's"*, IEEE Trans. Electron Devices ED-25, pp.825-832, 1978.

[10] A. Schultz, S. Selberrherr and H.W. Potzl, *"Numerical analysis of breakdown phenomena in MOSFET's"*, Proc. NASECODE II, Dublin, Boole Press, pp. 270-274, 1981.

[11] M. Reiser, *"A two-dimensional numerical FET model for DC, AC and large-signal analysis"*, IEEE Trans. Electron devices, ED-20, pp.35-44, 1973.

[12] C.M. Snowden, M.J. Howes and D.V. Morgan, *"Large signal modeling of GaAs MESFET's operation"*, IEEE Trans. Electron Devices, pp.817-1824, 1983.

[13] A. Husain and S.G. Chamberlain, *"Three-dimensional simulation of VLSI MOSFET's: The three-dimensional simulation program WATMOS"*, IEEE Trans. Electron Devices, ED-29, pp.631-638, 1982.

[14] A. Yoshii, M. Kitazawa, S Horigushi and T. Sudo, *"A three-dimensional analysis of semiconductor devices"*, IEEE Trans. Electron Devices, ED- 29, pp.184-189, 1982.

[15] S. Selberrherr, A. Schultz and H.W. Potzl, *"MINIMOS - a two-dimensional MOS transistor analyzer"*, IEEE Trans. Electron Devices, ED-27, pp.1540-1550, 1980.

[16] T. Toyabe and S. Asai, *"Analytical models of threshold voltage and breakdown voltage of short channel MOSFET's derived from two-dimensional analysis"*, IEEE Trans. Electron Devices, ED-26, pp.453-461.

[17] T.C. Denton, *"Validation of BIPOLE", Proc. 2nd International Conf. on Simulation of Semiconductor Devices and Processes"*, Swansea, Pineridge Press, pp.169-181, 1986.

[18] A.F. Franz, G.A. Franz, S. Selberrherr, C. Ringhofer and P. Markowich, *"Finite Boxes: - A generalization of the finite-difference method suitable for semiconductor device simulation"*, IEEE Trans. Electron Devices, ED-30, No. 9, pp.1070-1082. 1983.

[19] W. F. Ames, *"Numerical Methods for Partial Differential Equations"*, Academic Press, New York, 1977.

[20] U. Schultz and R. Pregla, *"A New Technique for the Analysis of the Dispersion Characteristics of Planar Waveguides"*, Arch. Eleck . Ubertragung, Vol.34, pp.169-173, 1980.

[21] S. Worm and R. Pregla, *"Hybrid Mode Analysis of Arbitrary Shaped Planar Microwave Structures by the Method of Lines"*, IEEE Trans. Microwave Theory Tach., Vol. MTT-32, No. 02, pp.191-196, 1984.

[22] U. Shultz, *"On the Edge Condition with the Method of Lines in Planar Waveguides"*, Arch. Eleck. Ubertragung, Vol.34, pp.176-178, 1980.

[23] R. pregla and W. Pascher, *"A Numerical Technique for Microwave and Millimeter Passive Structures"*, John Willey and Sons, 1989, Chapter 6.

[24] H. Diestel, *"Analysis of Planar Multiconductor Transmission-Line System with the Method of Lines"*, AEU Band 41, Heft 3, pp.169-175, 1987.

[25] R. Pregla *"About the Nature of the Method of Lines"*, Arch, Electron. Uebertragungs Tech., Vol. 41, Heft 6, pp.368-370, 1987.

[26] H. Diestel and S. B. Worm, *"Analysis of Hybrid Field Problems by the Method of Lines with Nonequidistant discretization"*, IEEE Trans. Microwave Theory Techn., Vol. MTT-32, No.6, pp.633-638, June 1984.

[27] R. Pregla, *"Analysis of Planar Microwave Structures on Magnetized Ferrite Substrate"*, AEU Band 40, pp. 270-274, Heft 5, 1986.

[28] R. Pregla, M. Koch, and W. Pasher, *"Analysis of Hybrid Waveguide Structure Consisting of Microstrips and Dielectric Waveguides"*, Proc. 17th European Microwave Conf., pp.927-932, Sept 1987.

[29] R. Pregla and W. Pasher, *"The Method of Lines"*, chap. 8 in *"Numerical techniques for microwave and millimeter wave passive structures"*, ed. T. Itoh, J. Wiley, 1989.

[30] A.G. Keen, M. I. Sobhy, *"An Adaptable Approach to the Analysis of Coplanar Multiconductor Slow-Wave Structures Using the Method of Lines"* Proc. 20th European Microwave Conf., pp.1340-1345, 1990, Budapest.

[31] Z. Q. Chen and B. X. Gao, *"New Approach to Analyzing Microstrip-Like Discontinuities in the MIC's Using the Method of Lines Demonstrated for End Effects"*, Electronic Letters, Vol.24, No.1, pp.2-4, January 1988.

[32] B. M. Sherrill and N. G Alexopoulous, *"The Method of Lines Applied to Finline Strip Configuration on Anisotropic Substrate"*, IEEE Trans. Microwave Theory Tech., Vol MTT-35, No.6, pp.568-574, June 1987.

[33] K. Wu and R. Vahldieck, *"The Method of Lines Applied to Planar Transmission Lines in Circular and Elliptical Waveguides"*, IEEE Trans. Microwave Theory Tech., Vol MTT-37, No.12, pp.1958-1963, December 1989.

[34] A. Issaoun, *"A Quasi-Static Analysis of MMIC Transmission-Line Structures by The Method of Lines"*, Magister Thesis, No. 01/92, INELEC, Boumerdes, Algeria.

[35] M. Affane, *"Multi-Dimensional Quasi-Static Analysis of MIC's and MMIC's "*, Magiser Thesis, No. 03/94, INELEC, Boumerdes, Algeria.

[36] A. Ouadi, *"Hybrid-mode Analysis of Microwave and Millimeter-wave Structures of Realistic Configurations "*, Magister Thesis, No. 02/95, INELEC, Boumerdes, Algeria.

[37] H. Bourdoucen, A. Zitouni and M. Dehmas, *"The Method of Lines Applied To The Analysis of Electrooptic Modulators"*, Proc. 4ème Colloque Maghrebin de L' Ingénieur, USTHB, Algeria, Vol.2, pp.375-379, 1993.

[38] C. M. Snowden, *"Introduction to Semiconductor Device modeling"*, World Scientific, 1986.

[39] Adir Bar-lev, *"Semiconductors and Electronic Devices"*, third edition, Prentice Hall International, 1993.

[40] R.S. Muller and T. L. Kamins, *"Device Electronics for Integrated Circuits"*, John Willey and Sons, 1977.

[41] Aldert van der Ziel, "*Solid State Physical Electronics*" third edition. Prentice-Hall, Inc., Englewood Cliffs, 1976.

[42] K. Kano, *"Physical and Solid State Electronics"*, Addison Wesley, Inc., 1972.

[43] C. M. Snowden, *"Semiconductor Device Modeling"*, Springer Verlag, 1989.

[44] Barnes, J.J. and Lomax, R.J.,, "Finite element methods in semiconductor device modeling ", IEEE Trans. Electron Devices ED-24, pp.1082-1089, 1977.

[45] Adachi, T., Yoshii, A., and Sudo, T., *"Two-dimensional semiconductor analysis using finite-element method"*, IEEE Trans. Electron Devices ED-26, pp.1026-1031, 1979.

[46] O. C. Zienkiewicz & K. Morgan, *"Finite element approximation"*, John Wiley & sons, 1983.

[47] Kurosawa, T., Proc. Int. Conf. on Physics of Semiconductors, Kyoto, (J. Phys., Soc. japan, 21, Suppl. p.527), 1966.

[48] M. Dehmas, A. Zitouni and H. Bourdoucen, *"A Seminumerical Technique for the Analysis of Integrated Semiconductor Devices"*, Modeling, Measurement & Control, A, Vol. 58, N° 2, pp.1-6, 1994.

[49] Erwin Kreyszig, *"Advanced Engineering Mathematics "*, John Wiley and Sons, 7th edition, 1993.

[50] J. H. Mathews, *"Numerical Methods for Mathematics, Science and Engineering"*, 2nd Edition, Prentice-Hall International Editions, 1992.

[51] P. Richman, *"MOS Field-Effect Transistors and Integrated Circuits"*, John Willey and Sons, 1973.

[52] B.G. Streetman, *"Solid State Electronic Devices"*, 3rd Edition, Prentice-Hall International Editions, 1990.

[53] G. Barbottin & A. Vapaille, *"Instabilities in Silicon Devices, silicon passivation and related instabilities"*, Elsevier science publishers, B.V North Holland, Vol. 1, 1986.

[54] B.L Palfrey and N.G Tarr, *" Introduction to Microelectronic Devices"*, Prentice-Hall International Editions, 1989.

[55] S. K. Ghandi, *"Semiconductor Power Devices"*, John Willey and Sons, 1977.

[56] A. Rusu and C. Bulucea, *"Deep-Depletion Breakdown Voltage of Silicon-Dioxide Silicon MOS Capacitors"*, IEEE Trans. Electron Devices, Vol. ED-26, No. 3, March 1979.

A N N E X

Liste et composition du Jury en vue de la soutenance de mémoire de Magister en Ingenierie des Systemes Electroniques par *Mr DAHMAS Mokrane.*

PRESIDENT/ *Dr A. FARAH,* Maitre de Conference, E N P

RAPPORTEUR/ *Dr H. BOURDOUCEN*, Maitre de Conference, I N E L E C

MEMBRES/ *Dr R. AKSAS,* Maitre de Conference, E N P
Dr MT. BELLAROUSSI PhD, Charge de Recherche, C D T A
Dr M. BOUMAOUR, PhD Chargé de Recherche, U D T S